A discontinuous Galerkin method for linear symmetric hyperbolic systems in inhomogeneous media

Peter Monk* Gerard R. Richter †

August 4, 2003

Abstract

The Discontinuous Galerkin (DG) method provides a powerful tool for approximating hyperbolic problems. Here we derive a new space-time DG method for linear time dependent hyperbolic problems written as a symmetric system (including the wave equation and Maxwell's equations). The main features of the scheme are that it can handle inhomogeneous media, and can be time-stepped by solving a sequence of small linear systems resulting from applying the method on small collections of space-time elements. We show that the method is stable provided the space-time grid is appropriately constructed (this corresponds to the usual time-step restriction for explicit methods, but applied locally) and give an error analysis of the scheme. We also provide some simple numerical tests of the algorithm applied to the wave equation in two space dimensions (plus time).

1 Introduction

The Discontinuous Galerkin (DG) method was first proposed in 1973 [13] for approximating the scalar neutron transport equation. Since then the method has been analyzed (see [11, 10] for an analysis of the original method) and extended to a wide range of applications. In particular, for time dependent problems, the usual approach is to use a method of lines by first using the DG scheme to approximate the problem in space and then to apply an appropriate time-stepping scheme to the resulting system of differential equations. A particularly powerful combination is to apply the DG method in space and a Runge-Kutta scheme in time to obtain an RKDG scheme (see [1]). This philosophy has been used by Hesthaven and Warburton [7] to implement a high order (up to 10th degree piecewise polynomials in space) RKDG scheme for

*Department of Mathematical Sciences, University of Delaware, Newark DE 19716, USA

†Computer Science Department, Rutgers University, Busch Campus, Piscataway NJ 08854-8019, USA

Maxwell's equations. Furthermore, the method uses a tetrahedral spatial grid to provide good geometric approximation. The spatial DG approach can also be used to couple blocks in pseudospectral codes (see [2] for Maxwell's equations). In addition, finite volume schemes can be viewed as low order DG schemes, and this observation is used to prove convergence results for an explicit finite volume method for first order systems in [16].

One disadvantage of the RKDG and explicit finite volume approaches is that the time step is governed by the smallest elements in the mesh via a CFL condition. For grids that are refined to fit geometric features or to control error in the discrete solution, such methods can become very time consuming.

The explicit time step (or CFL) constraint can be avoided. For example, Hughes and Hulbert [9] suggest using a space time grid formed by the tensor product of a spatial grid and a time grid. A DG scheme in space and time is then applied to obtain an implicit discretization of a hyperbolic problem necessitating the solution of a large linear system at each timestep.

Methods such as those discussed above using DG in space can easily incorporate spatially varying coefficients resulting from an inhomogeneous medium. This is desirable since such media often arise in practice. For example, acoustic waves impinging on a penetrable object such as the human torso (i.e., waves due to an ultrasound source) encounter differing acoustic properties in the body.

Our goal is to obtain a semi-explicit method for time-stepping the acoustic wave equation or Maxwell's equations written in symmetric hyperbolic form. By semi-explicit, we mean that only matrix problems derived from small or local collections of elements need to be solved. In addition, we want to be able to take time-steps controlled by a local CFL condition (i.e., larger time-steps for larger elements). Finally, we want the method to handle inhomogeneous media.

The approach we take is motivated by the work of Falk and Richter [5] who proposed an explicit discontinuous Galerkin method for symmetric hyperbolic systems with smooth coefficients. In particular, we extend their space-time discontinuous Galerkin method to one which generates a piecewise polynomial approximation over individual simplices, as opposed to more the complex polyhedra used in [5]. We then show how this extension allows us to treat a class of inhomogeneous medium problems involving discontinuous coefficients, and how it can be timestepped by solving only local problems with a locally determined stabilty constraint.

The layout of the paper is as follows. In the next section (Section 2), we give details of the symmetric system we propose to solve and present the discontinuous Galerkin method. In Section 3 we discuss our mesh assumptions and briefly comment on how to generate an appropriate mesh using an advancing front technique for unstructured grids analyzed in [4]. Next, in Section 4 we derive some stability estimates for the discrete problem, and prove existence and uniqueness of the discrete solution. We then prove various error bounds for the solution in Section 5. Some of these bounds require more specialized assumptions (satisfied by the grids we use) than those outlined in Section 2. The symmetric Friedrichs system imposes boundary data via an auxilliary matrix function on the boundary. In Section 6 we show how to construct a fairly

general class of boundary matrices for the acoustic wave equation which will be the example used in our numerical experiments in Section 7. Finally, in Section 8 we summarize our experience with this method and future plans.

2 Symmetric Hyperbolic Systems

Suppose Ω is a bounded Lipschitz polyhedral domain in $\mathbb{R}^N$, $N \geq 1$, and let $\boldsymbol{u}$ denote an m-vector function of position $\boldsymbol{x} \in \Omega$ and time $t \in (0,T]$ (i.e. $\boldsymbol{u}(\boldsymbol{x},t) \in \mathbb{R}^m$) which satisfies the symmetric hyperbolic system

$$\mathcal{L}\boldsymbol{u} \equiv A\boldsymbol{u}_t + \sum_{j=1}^{N} A_j \boldsymbol{u}_{x_j} + B\boldsymbol{u} = \boldsymbol{f} \quad \text{in } \Omega_T = \Omega \times (0,T]. \tag{1}$$

Here the subscripts t and x_j denote partial differentiation, and A, A_j and B are $m \times m$ matrices, all assumed to be to be symmetric and independent of time. In addition, we assume that A is positive definite and piecewise constant over a polyhedral subdivision of Ω, that A_j, $j = 1, ...N$ are constant, and that B is positive semi-definite with entries in $L^\infty(\Omega)$. These assumptions are motivated by the problems we wish to solve, in acoustics and electromagnetism, and a desire to avoid nonessential details in our analysis.

On a (hyper)planar surface S in the space-time domain with normal $\boldsymbol{n} = (n_t, n_1, ..., n_N)^T$, the quantity $\mathsf{M}\boldsymbol{u}$,

$$\mathsf{M} = n_t A + \sum_{j=1}^{N} n_j A_j, \tag{2}$$

plays the role of a flux across S in the direction of $\boldsymbol{n}$. Taking S to be the interface where A is discontinuous, we have $n_t = 0$ and M becomes

$$D = \sum_{j=1}^{N} n_j A_j,$$

which is well-defined on S apart from sign (corresponding to the two possible orientations of $\boldsymbol{n}$) since the A_j's are continuous. Accordingly, we require that the jump in $\boldsymbol{u}$ across the interface, denoted $[\boldsymbol{u}]$, satisfy $D[\boldsymbol{u}] = 0$. It follows that $[\boldsymbol{u}^T D\boldsymbol{u}] = 0$ also. For the applications of interest to us, D is singular on such interfaces (characteristic surfaces); thus discontinuous solutions are anticipated.

We augment the symmetric system (1) by the initial condition

$$\boldsymbol{u} = \boldsymbol{u}_0 \quad \text{for } t = 0 \text{ and } \boldsymbol{x} \in \Omega \tag{3}$$

where $\boldsymbol{u}_0$ is a given function, and by boundary conditions of the form

$$(D - \mathsf{N})\boldsymbol{u} = \boldsymbol{g} \quad \text{on } \Gamma \times (0,T]. \tag{4}$$

Here Γ denotes the boundary of Ω, D is formed as above using the components of the spatial unit outward normal $\boldsymbol{n}_x = (n_1, n_2, \ldots, n_N)^T \in \mathbb{R}^N$ to Γ, N is a

piecewise constant $m \times m$ matrix function of position, and $\boldsymbol{g}$ is an appropriate given vector function (for a discussion of boundary conditions for the wave equation see Section 6). The matrix N is chosen so that (4) is equivalent to whatever is the desired boundary condition. It is not unique, but for Friedrichs' theory of symmetric hyperbolic systems [6], it must satisfy the following two conditions,

$$\begin{aligned} \mathsf{N} + \mathsf{N}^T &\geq 0 \quad \text{on } \Gamma \times (0,T], && (5) \\ \ker(D - \mathsf{N}) + \ker(D + \mathsf{N}) &= \mathbb{R}^m \quad \text{on } \Gamma \times (0,T]. && (6) \end{aligned}$$

Of these conditions, only the first is used directly in our finite element analysis. In this analysis, we shall assume $\boldsymbol{f} \in (L^2(\Omega_T))^m$, $\boldsymbol{u}_0 \in (L^2(\Omega))^m$, and $\boldsymbol{g} \in (L^2(\Gamma))^m$.

The initial-boundary value problem (1),(3),(4) satisfies an energy equality. Writing $\Omega = \cup_{\ell=1}^{L} \Omega_\ell$ where A is constant in each Ω_ℓ, suppose $\boldsymbol{g} = 0$ and $\boldsymbol{f} = 0$. Then multiplying the equation (1) by $\boldsymbol{u}^T$ and integrating over Ω_T, we obtain

$$\begin{aligned} 0 &= \sum_{\ell=1}^{L} \int_{\Omega_\ell \times [0,T]} \boldsymbol{u}^T (A\boldsymbol{u}_t + \sum_{j=1}^{N} A_j \boldsymbol{u}_{x_j} + B\boldsymbol{u})\, d\sigma \\ &= \frac{1}{2} \left\{ \int_\Omega \left(\boldsymbol{u}^T(T) A \boldsymbol{u}(T) - \boldsymbol{u}^T(0) A \boldsymbol{u}(0) \right) dV + \sum_{\ell=1}^{L} \int_0^T \left(\int_{\Gamma(\Omega_\ell)} \boldsymbol{u}^T D \boldsymbol{u}\, dA \right) dt \right\} \\ &\quad + \int_{\Omega_T} \boldsymbol{u}^T B \boldsymbol{u}\, d\sigma. \end{aligned}$$

Applying the jump condition $D[\boldsymbol{u}] = 0$, integrals over interior surfaces $\Gamma(\Omega_\ell)$ cancel one another. Thus using the boundary condition (4) and collecting terms, we obtain

$$\begin{aligned} \int_\Omega \boldsymbol{u}^T(T) A \boldsymbol{u}(T)\, dV &+ \int_0^T \left(\int_\Gamma \boldsymbol{u}^T \mathsf{N} \boldsymbol{u}\, dA \right) dt + 2 \int_{\Omega_T} \boldsymbol{u}^T B \boldsymbol{u}\, d\sigma \\ &= \int_\Omega \boldsymbol{u}^T(0) A \boldsymbol{u}(0)\, dV. \end{aligned}$$

Since the symmetric part of N is positive semi-definite and B is positive semi-definite, we obtain the basic energy inequality

$$\int_\Omega \boldsymbol{u}^T(T) A \boldsymbol{u}(T)\, dV \leq \int_\Omega \boldsymbol{u}^T(0) A \boldsymbol{u}(0)\, dV,$$

which our finite element method will preserve.

The discontinous Galerkin method we propose in this paper uses a family of regular finite element meshes $\{\tau_h\}_{h>0}$, each consisting of $(N+1)$-simplices of maximum diameter h covering the space-time domain Ω_T. We denote the diameter of a simplex $K \in \tau_h$ by h_K and the diameter of its largest inscribed sphere (or hypersphere) by ρ_K. The condition that $\{\tau_h\}$ is regular means that there exists a constant C independent of K and τ_h such that

$$\frac{h_K}{\rho_K} \leq C \text{ for all } K \in \tau_h \text{ and all } \tau_h.$$

To facilitate construction of a numerical scheme with high order accuracy in the vicinity of discontinuities, we require all discontinuities in A and N to lie on element boundaries (not possible for the method of [5], which requires element boundaries in the interior of Ω_T to be inflow or outflow, as described below).

We denote the boundary of a space-time element K by $\Gamma(K)$ and its unit outward normal by $\boldsymbol{n} = \begin{pmatrix} n_t \\ \boldsymbol{n}_x \end{pmatrix}$ where $\boldsymbol{n}_x$ is the spatial part of the normal. It will be convenient to divide $\Gamma(K)$ into its exterior faces

$$\Gamma_e(K) = \Gamma(K) \cap (\Gamma \times [0,T]) \tag{7}$$

and its interior faces

$$\Gamma_i(K) = \Gamma(K) \setminus \Gamma_e(K), \tag{8}$$

and extend these definitions to more general polyhedra in the obvious way. In addition, we use the notation

$$(\boldsymbol{u},\boldsymbol{v})_K = \int_K \boldsymbol{u}\cdot\boldsymbol{v}\,dV, \qquad \langle \boldsymbol{u},\boldsymbol{v}\rangle_S = \int_S \boldsymbol{u}\cdot\boldsymbol{v}\,dA, \tag{9}$$

where S consists of one or more faces of $\Gamma(K)$. Also, we denote the $H^p(K)$ and $H^p(S)$ norms by $\|\cdot\|_{p,K}$ and $|\cdot|_{p,S}$, with p omitted when it has value zero.

The following integration by parts identity, valid for differentiable functions $\boldsymbol{u}$ and $\boldsymbol{v}$, underlies our method:

$$(\mathcal{L}\boldsymbol{u},\boldsymbol{v})_K = -(\boldsymbol{u},\mathcal{L}\boldsymbol{v})_K + 2(B\boldsymbol{u},\boldsymbol{v})_K + \langle \boldsymbol{u},\mathsf{M}\boldsymbol{v}\rangle_{\Gamma(K)}, \tag{10}$$

where M is as in (2). We decompose M into a sum $\mathsf{M} = \mathsf{M}^+ + \mathsf{M}^-$ of symmetric matrices where M^+ is positive semi-definite, and M^- is negative semi-definite. In general this decomposition is not unique, but we adopt the rule that if M itself is semi-definite, then we always take one of the summands $\mathsf{M}^\pm$ to be zero. In the case where M is indefinite, a classical way to obtain such a splitting is to write $\mathsf{M} = Q(\Lambda^+ + \Lambda^-)Q^T$ where Q is an orthogonal matrix of eigenvectors of M and Λ^+ and Λ^- are diagonal matrices having, respectively, the positive and negative eigenvalues of M on the main diagonal. Then we take $\mathsf{M}^+ = Q\Lambda^+Q^T$ and $\mathsf{M}^- = Q\Lambda^-Q^T$. Although this choice is sufficient for theoretical purposes, other choices of M^+ and M^- are possible provided the null spaces of $\mathsf{M}^+ - \mathsf{M}^-$ and M are identical. The best choice of M^+ for wave propagation is an open problem [8], and we shall describe the splitting used in this paper for the acoustic wave equation in Section 6 (only in the case $n_t = 0$ since that is all our algorithm will require).

Since M is piecewise constant on element boundaries under our mesh assumptions, we may categorize the faces of K as follows:

- M is negative definite (so $\mathsf{M} = \mathsf{M}^-$). The set of all faces in $\Gamma_i(K)$ on which M is negative definite is called the "inflow boundary" for K and denoted $\Gamma_{\text{in}}(K)$.

- M is positive definite (so $\mathsf{M} = \mathsf{M}^+$). The set of all faces in $\Gamma_i(K)$ on which M is positive definite is called the "outflow boundary" for K and denoted $\Gamma_{\text{out}}(K)$.

- M is indefinite. The set all faces of $\Gamma_i(K)$ on which M is indefinite is denoted $\Gamma_{\rm ind}(K)$.

We note that on $\Gamma_e(K)$, M reduces to D which for our applications is always indefinite, though it need not be so in general. In addition, we extend the definitions of $\Gamma_{in}, \Gamma_{out}$, and $\Gamma_{\rm ind}$ to a union of simplices in the obvious way, e.g., $\Gamma_{\rm in}(K_1 \cup K_2)$ is the portion of $\Gamma(K_1 \cup K_2)$ where M is negative definite.

On an element K, we define the fundamental bilinear form for the method by

$$\begin{aligned} a_K(\boldsymbol{u},\boldsymbol{v}) &= -(\boldsymbol{u},\mathcal{L}\boldsymbol{v})_K + 2(B\boldsymbol{u},\boldsymbol{v})_K + \langle \boldsymbol{u}, \mathsf{M}^+\boldsymbol{v}\rangle_{\Gamma_i(K)} \\ &\quad + \langle \boldsymbol{u}_{\rm ext}, \mathsf{M}^-\boldsymbol{v}\rangle_{\Gamma_i(K)} + \frac{1}{2}\langle (\mathsf{N}+D)\boldsymbol{u},\boldsymbol{v}\rangle_{\Gamma_e(K)}, \end{aligned} \tag{11}$$

where $\boldsymbol{u},\boldsymbol{v} \in (H^1(K))^m$ and $\boldsymbol{u}_{\rm ext}$ is the value of $\boldsymbol{u}$ on the adjoining simplices exterior to K. Equivalently, using (10) we may write this as

$$a_K(\boldsymbol{u},\boldsymbol{v}) = (\mathcal{L}\boldsymbol{u},\boldsymbol{v})_K + \langle \mathsf{M}^-(\boldsymbol{u}_{\rm ext}-\boldsymbol{u}),\boldsymbol{v}\rangle_{\Gamma_i(K)} + \frac{1}{2}\langle (\mathsf{N}-D)\boldsymbol{u},\boldsymbol{v}\rangle_{\Gamma_e(K)}. \tag{12}$$

If a face of $\Gamma(K)$ lies on the initial $t=0$ surface then $\boldsymbol{u}_{\rm ext}$ is given by the initial data (3). On K, an exact solution $\boldsymbol{u} \in (H^1(K))^m$ of (1),(3),(4) together with the interface condition $D[\boldsymbol{u}] = 0$ satisfies

$$a_K(\boldsymbol{u},\boldsymbol{v}) = (\boldsymbol{f},\boldsymbol{v})_K - \frac{1}{2}\langle \boldsymbol{g},\boldsymbol{v}\rangle_{\Gamma_e(K)} \tag{13}$$

for all $\boldsymbol{v} \in (H^1(K))^m$.

The numerical scheme is now obvious. Let $P_p(K)$ denote the set of polynomials of maximum degree at most p in $(t, x_1, \cdots, x_N)$. We seek $\boldsymbol{u}_h$ such that $\boldsymbol{u}_h|_K \in (P_p(K))^m$ for each element $K \in \tau_h$ and such that

$$a_K(\boldsymbol{u}_h,\boldsymbol{v}_h) = (\boldsymbol{f},\boldsymbol{v}_h)_K - \frac{1}{2}\langle \boldsymbol{g},\boldsymbol{v}_h\rangle_{\Gamma_e(K)} \tag{14}$$

for all $\boldsymbol{v}_h \in (P_p(K))^m$. At $t=0$, $\boldsymbol{u}_{h,\rm ext}$ is taken to be the $(L^2(\Omega))^m$ projection of $\boldsymbol{u}_0$ (this can be computed element by element). If the initial data is smooth, the interpolant can alternatively be used.

3 The Space-Time Grid

In general, use of (14) with an arbitrary space-time grid will result in a coupled system of equations over the entire space-time region that must be solved simultaneously. However, for an appropriately generated mesh, the solution procedure can be reduced to a semi-explicit process, involving a sequence of local problems on small groups of elements termed "macroelements". Our additional mesh requirements are as follows:

- The simplices in τ_h can be grouped into non-overlapping macroelements $\{\tilde{K}\}$, each a union of a uniformly bounded (independent of h) number

of simplices, with the property that the macroelements can be ordered explicitly with respect to domain of dependence. By this we mean the macroelements can be ordered $\tilde{K}_1, \tilde{K}_2, \ldots$ such that

$$\Gamma_{\text{in}}(\tilde{K}_i) \subset \Gamma_{\text{in}}(\Omega_T) \cup \Gamma_{\text{out}}(\cup_{j<i} \tilde{K}_j).$$

(Thus $\Gamma_{\text{ind}}(\tilde{K}) = \emptyset$ for each macroelement.) In general, a space-time mesh which admits such an ordering will admit many such orderings, but the solution is independent of the choice of the ordering.

- The mesh is locally quasi-uniform in the sense that the ratio $\max_{K \subset \tilde{K}} h_K / \min_{K \subset \tilde{K}} h_K$ is bounded away from zero and infinity, independent of $\tilde{K}$ and the mesh τ_h to which $\tilde{K}$ belongs.

Since the solution on a given element is only coupled to other elements via indefinite surfaces ($\Gamma_{\text{ind}}(K)$) or inflow boundaries ($\Gamma_{\text{in}}(K)$) we see that the ordering assumption implies we can solve the discrete problem successively first on $\tilde{K}_1$, then on $\tilde{K}_2$, etc.

Note that the assumption of an explicit ordering imposes a CFL like time step restriction. A face is an outflow face of an element K if $\mathsf{M} = \mathsf{M}^+$ there. Since $\mathsf{M} = An_t + D$ and A is positive definite, we see that a face with normal $(n_t, n_1, \ldots, n_N)$ will be an outflow face if n_t is suffiently close to $+1$. The time-stepping scheme chooses the elements in order to satisfy the explicit ordering assumption with a time-step that keeps the grid regular (so very flat elements are avoided).

We also make two additional stipulations on the mesh that we shall use in our analysis:

- The eigenvalues $\lambda(\mathsf{M})$ of M are uniformly bounded away from zero on all inflow and outflow boundaries. This, together with the upper bound $\lambda(\mathsf{M}) \leq \sqrt{\rho(A)^2 + \sum_j \rho(A_j)^2}$, will imply that our error estimates in terms of weighted norms involving M are equivalent to standard Sobolev norms.

- For each simplex $K \subset \tilde{K}$, $\Gamma_e(K)$ consists of at most one face, and $\Gamma(K)$ has a nonempty intersection with $\Gamma_{\text{in}}(\tilde{K}) \cup \Gamma_{\text{out}}(\tilde{K})$.

We now address the question of how to generate a desirable grid which satisfies the assumptions we have imposed. One possible approach would be to produce a regular and quasi-uniform grid of the entire space-time domain at the start of the algorithm. Indeed this is the way we have presented the method so far. However such a grid would be expensive to store (in $3+1$ dimensions for example) and the ordering assumption given above would be difficult to satisfy using a standard mesh generator.

Instead of pre-computing the grid on the entire space-time region we develop the space-time grid macroelement by macroelement during the solution procedure using an advancing front approach termed "tent-pitching". This method was used by Falk and Richter [5] for uniform grids and developed for non-uniform grids by Üngör and Sheffer [15] and Erickson et al. [4]. We follow

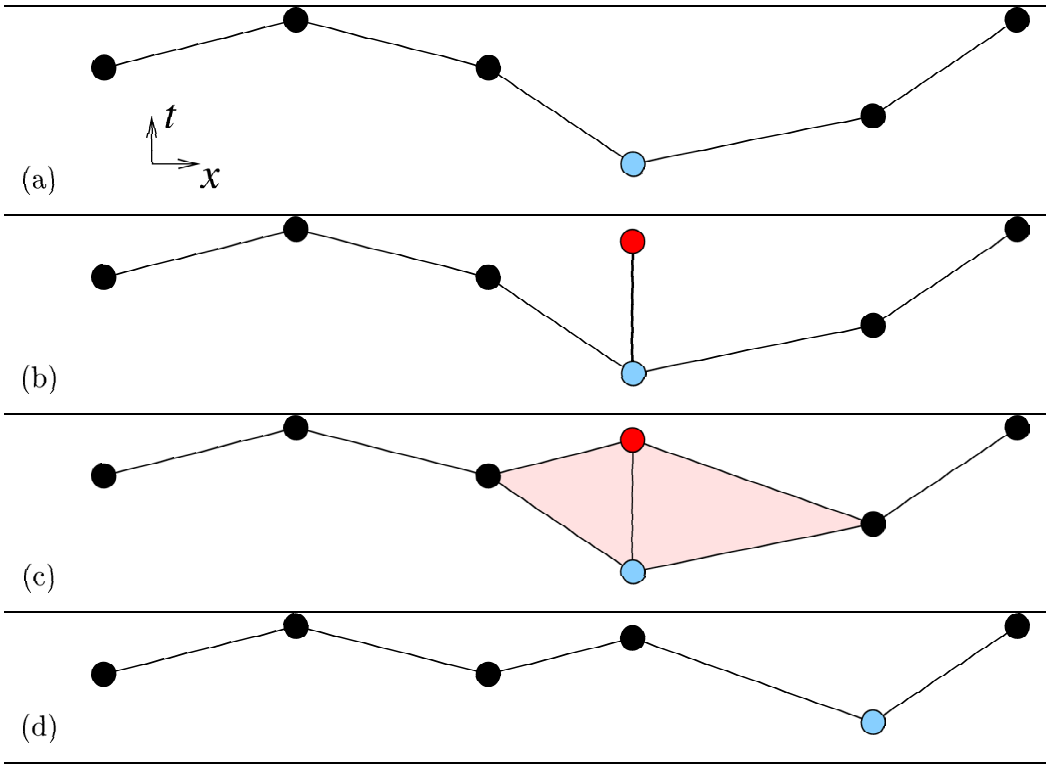

Figure 1: Here we show a sequence of grid fronts to explain the tent pitching algorithm. The top panel shows the current grid front (in one space dimension plus time). The lowest vertex is chosen to be moved forward in time (lightly shaded point). Panel (b) shows the vertical tent pole erected at the lowest vertex (the algorithm ensures that this vertex can move past the lowest of its neighbors). In panel (c) we show the macroelement consisting of two triangles in space-time meeting at the tent pole. After solving the discrete equations on this macroelement the solution is now known on the upper part of the grid. Hence the macroelement can be deleted and the the updated grid front is shown in panel (d) ready for the next vertex to be moved ahead.

the latter paper and now give a brief description of the procedure (for a cartoon of the steps of the method when $N = 1$ see Fig. 1).

In the present paper we shall only show two space dimensional results. Thus we first generate a grid for $\Omega \subset \mathbb{R}^2$ using the MATLAB PDETool mesh generator. This forms the spatial grid at $t = 0$ (so at the start all vertices are assigned time $t = 0$). At any step of the algorithm we store a space-time grid front which has the same connectivity as the original mesh at $t = 0$ but with vertices at possibly different times (see Fig. 1 a). The space-time grid front is then updated as follows. Using the "lowest vertex first" criterion from [4] we choose a vertex having the lowest time and create an edge forward in time from that vertex to a new vertex in the space-time grid (erect a tent-pole – see Fig. 1 b). A space-time macroelement is then formed by all the tetrahedra whose vertex set includes the vertices of the tent-pole and the vertices of a triangle in the current space-time mesh touching the base of the tent-pole (see Fig. 1 c). The height of the tent-pole is chosen so that the faces of the macroelement meeting at the top of the tent-pole are outflow. In general one would like to take the tallest tent-pole consistent with having all upper faces as outflow (in particular so that the uniformity condition on $\lambda(\mathsf{M})$ is satisfied), but it is easy to see that, in higher dimensions, this can prevent tents from being erected at surrounding vertices. Therefore the tent-pole must be chosen short enough to allow surrounding tents to be erected and we follow the criterion of [4]. Once the macroelement is formed, the finite element solution can be computed on the macroelement. The solution is then known along the outflow surface of the macro-element so it is recorded, the space-time front is updated by replacing the vertex at the base of the tent-pole by the one at the top (moving ahead in time) and the macroelement is discarded (see Fig. 1 d.). Thus only the space-time grid front and the solution on this front are stored within the algorithm, so reducing memory needs compared to an implicit method over the whole domain. Note that the length of the tent-pole (the local time-step) is governed by the geometry of the elements meeting at its base (and the local parameter values of the hyperbolic system) and the time-step is not dictated globally by the smallest elements in the mesh.

Clearly this method produces macroelements having a number of tetrahedra equal to the number of triangles meeting at a vertex (bounded uniformly in h since the initial spatial grid is regular). All the external faces meeting at the bottom of the tent-pole are inflow and all the faces meeting at the top of the pole are outflow (or boundary) faces. Indefinite faces all have $n_t = 0$ and so $\mathsf{M} = D$ there. Note that it is proved in [4], Theorem 3 that the resulting space-time grid is regular.

4 Uniqueness and Stability

In this section we derive some stability results for the discontinuous Galerkin method, and show that there exists a unique solution to the discrete problem (14). Our most basic result is:

Lemma 1 *If $\boldsymbol{u}|_K \in (H^1(K))^m$ for all $K \in \tau_h$, the following equality holds on each element K in the space-time mesh.*

$$\begin{aligned} a_K(\boldsymbol{u},\boldsymbol{u}) &= \frac{1}{2}\left\{\langle \boldsymbol{u}, \mathsf{M}^+\boldsymbol{u}\rangle_{\Gamma_i(K)} + \langle \boldsymbol{u}_{\rm ext}, \mathsf{M}^-\boldsymbol{u}_{\rm ext}\rangle_{\Gamma_i(K)}\right. \\ &\quad \left. -\langle [\boldsymbol{u}], \mathsf{M}^-[\boldsymbol{u}]\rangle_{\Gamma_i(K)} + 2\,(B\boldsymbol{u},\boldsymbol{u})_K + \langle \mathsf{N}\boldsymbol{u},\boldsymbol{u}\rangle_{\Gamma_e(K)}\right\} \end{aligned} \tag{15}$$

where $[\boldsymbol{u}] = \boldsymbol{u}_{\rm ext} - \boldsymbol{u}$.

Proof
Using (11) with $\boldsymbol{u}$ and $\boldsymbol{v}$ interchanged and (12) we get

$$\begin{aligned} a_K(\boldsymbol{v},\boldsymbol{u}) + a_K(\boldsymbol{u},\boldsymbol{v}) &= 2\,(B\boldsymbol{v},\boldsymbol{u})_K + \langle \boldsymbol{v}, \mathsf{M}^+\boldsymbol{u}\rangle_{\Gamma_i(K)} + \langle \boldsymbol{v}_{\rm ext}, \mathsf{M}^-\boldsymbol{u}_{\rm ext}\rangle_{\Gamma_i(K)} \\ &\quad -\langle (\boldsymbol{v}_{\rm ext} - \boldsymbol{v}), \mathsf{M}^-(\boldsymbol{u}_{\rm ext} - \boldsymbol{u})\rangle_{\Gamma_i(K)} + \langle \mathsf{N}\boldsymbol{v},\boldsymbol{u}\rangle_{\Gamma_e(K)}. \end{aligned}$$

Taking $\boldsymbol{u} = \boldsymbol{v}$ completes the proof.

We now wish to analyze the bilinear form over a macroelement $\tilde{K}$. We define

$$a_{\tilde{K}}(\boldsymbol{u},\boldsymbol{v}) = \sum_{K\subset\tilde{K}} a_K(\boldsymbol{u},\boldsymbol{v})$$

and enumerate the elements in the macroelement by $K_1, K_2, \ldots$. For a pair of elements K_i and K_j in $\tilde{K}$ we define

$$\begin{aligned} &\Gamma_{i,j} = \Gamma(K_i) \cap \Gamma(K_j), \\ &G(\tilde{K}) = \cup_{K_i,K_j\subset\tilde{K}} \Gamma_{i,j}. \end{aligned}$$

Thus $G(\tilde{K})$ is the set of internal, or hidden, faces of $\tilde{K}$. Assuming $\Gamma_{i,j} \neq \emptyset$, the matrices D for K_i and K_j on $\Gamma_{i,j}$ have the opposite sign. The same is also true of $n_t A$, for discontinuities in A are confined to vertical interelement boundaries where $n_t = 0$. Thus on $\Gamma_{i,j}$ the corresponding matrices $\mathsf{M}_i, \mathsf{M}_j$ for K_i and K_j must satisfy

$$\mathsf{M}_i + \mathsf{M}_j = 0. \tag{16}$$

If the splittings of M_i and M_j are consistent on $\Gamma_{i,j}$, which we shall always assume to be the case, then on $\Gamma_{i,j}$ we have

$$\mathsf{M}_i^+ + \mathsf{M}_j^- = 0, \quad \mathsf{M}_i^- + \mathsf{M}_j^+ = 0. \tag{17}$$

Thus

$$\mathsf{M}_i^+ - \mathsf{M}_i^- = \mathsf{M}_j^+ - \mathsf{M}_j^-. \tag{18}$$

We now define a matrix $\mathcal{M}$ on $\Gamma(\tilde{K}) \cup G(\tilde{K})$ by

$$\mathcal{M} = \mathsf{M}^+ - \mathsf{M}^-. \tag{19}$$

Note that $\mathcal{M}$ is well-defined on $G(\tilde{K})$ in view of (18), as well as on macroelement boundaries, and that it is positive definite on $\Gamma(\tilde{K})$ and positive semi-definite on $G(\tilde{K})$.

We can now prove the following stability result for a single macroelement.

Lemma 2 *If* $\boldsymbol{u}|_K \in (H^1(K))^m$ *for all elements* $K \in \tau_h$, *then for each macroelement* $\tilde{K}$,

$$\begin{aligned} a_{\tilde{K}}(\boldsymbol{u},\boldsymbol{u}) &= \frac{1}{2}\Big\{\langle \boldsymbol{u}, \mathcal{M}\boldsymbol{u}\rangle_{\Gamma_{\rm out}(\tilde{K})} - \langle \boldsymbol{u}_{\rm ext}, \mathcal{M}\boldsymbol{u}_{\rm ext}\rangle_{\Gamma_{\rm in}(\tilde{K})} + \langle [\boldsymbol{u}], \mathcal{M}[\boldsymbol{u}]\rangle_{\Gamma_{\rm in}(\tilde{K})\cup G(\tilde{K})} \\ &\quad + 2\,(B\boldsymbol{u},\boldsymbol{u})_{\tilde{K}} + \langle \boldsymbol{u}, \mathsf{N}\boldsymbol{u}\rangle_{\Gamma_e(\tilde{K})}\Big\}. \end{aligned} \tag{20}$$

Proof
Adding (15) over the elements K of $\tilde{K}$ we obtain

$$\begin{aligned} a_{\tilde{K}}(\boldsymbol{u},\boldsymbol{u}) &= \frac{1}{2}\Big\{\langle \boldsymbol{u}, \mathsf{M}^+\boldsymbol{u}\rangle_{\Gamma_{\rm out}(\tilde{K})} + \langle \boldsymbol{u}_{\rm ext}, \mathsf{M}^-\boldsymbol{u}_{\rm ext}\rangle_{\Gamma_{\rm in}(\tilde{K})} - \langle [\boldsymbol{u}], \mathsf{M}^-[\boldsymbol{u}]\rangle_{\Gamma_{\rm in}(\tilde{K})} \\ &\quad + \sum_{\Gamma_{i,j}\in G(\tilde{K}),\, i<j} \Big\{\langle \boldsymbol{u}_i, \mathsf{M}_i^+\boldsymbol{u}_i\rangle_{\Gamma_{i,j}} + \langle \boldsymbol{u}_j, \mathsf{M}_i^-\boldsymbol{u}_j\rangle_{\Gamma_{i,j}} - \langle [\boldsymbol{u}], \mathsf{M}_i^-[\boldsymbol{u}]\rangle_{\Gamma_{i,j}} \\ &\qquad + \langle \boldsymbol{u}_j, \mathsf{M}_j^+\boldsymbol{u}_j\rangle_{\Gamma_{i,j}} + \langle \boldsymbol{u}_i, \mathsf{M}_j^-\boldsymbol{u}_i\rangle_{\Gamma_{i,j}} - \langle [\boldsymbol{u}], \mathsf{M}_j^-[\boldsymbol{u}]\rangle_{\Gamma_{i,j}}\Big\} \\ &\quad + 2\,(B\boldsymbol{u},\boldsymbol{u})_{\tilde{K}} + \langle \mathsf{N}\boldsymbol{u}, \boldsymbol{u}\rangle_{\Gamma_e(\tilde{K})}\Big\} \end{aligned} \tag{21}$$

Now using the equalities in (16)–(18) we see that that

$$\begin{aligned} \langle \boldsymbol{u}_i, \mathsf{M}_i^+\boldsymbol{u}_i\rangle_{\Gamma_{i,j}} &+ \langle \boldsymbol{u}_j, \mathsf{M}_i^-\boldsymbol{u}_j\rangle_{\Gamma_{i,j}} - \langle [\boldsymbol{u}], \mathsf{M}_j^-[\boldsymbol{u}]\rangle_{\Gamma_{i,j}} \\ &+ \langle \boldsymbol{u}_j, \mathsf{M}_j^+\boldsymbol{u}_j\rangle_{\Gamma_{i,j}} + \langle \boldsymbol{u}_i, \mathsf{M}_j^-\boldsymbol{u}_i\rangle_{\Gamma_{i,j}} - \langle [\boldsymbol{u}], \mathsf{M}_i^-[\boldsymbol{u}]\rangle_{\Gamma_{i,j}} \\ &= \langle [\boldsymbol{u}], (\mathsf{M}_i^+ - \mathsf{M}_i^-)[\boldsymbol{u}]\rangle_{\Gamma_{i,j}}. \end{aligned}$$

Use of this equality in (21) and the definition of $\mathcal{M}$ completes the proof.

One more equality is needed before presenting the discretization of the method. This provides an expansion for the general bilinear form on a macroelement.

Lemma 3 *If* $\boldsymbol{u}|_K$, $\boldsymbol{v}|_K \in (H^1(K))^m$ *for all* $K \in \tau_h$, *then for each macroelement* $\tilde{K}$,

$$\begin{aligned} a_{\tilde{K}}(\boldsymbol{u},\boldsymbol{v}) &= -\sum_{K\subset\tilde{K}} (\boldsymbol{u}, \mathcal{L}\boldsymbol{v})_K + \langle \boldsymbol{u}, \mathcal{M}\boldsymbol{v}\rangle_{\Gamma_{\rm out}(\tilde{K})} \\ &\quad - \langle \boldsymbol{u}_{\rm ext}, \mathcal{M}\boldsymbol{v}_{\rm ext}\rangle_{\Gamma_{\rm in}(\tilde{K})} + \langle \boldsymbol{u}_{\rm ext}, \mathcal{M}[\boldsymbol{v}]\rangle_{\Gamma_{\rm in}(\tilde{K})} \\ &\quad + \sum_{\Gamma_{i,j}\in G(\tilde{K}),\, i<j} \Big\{\langle \boldsymbol{u}_j, \mathsf{M}_i^-(\boldsymbol{v}_i - \boldsymbol{v}_j)\rangle_{\Gamma_{i,j}} + \langle \boldsymbol{u}_i, \mathsf{M}_j^-(\boldsymbol{v}_j - \boldsymbol{v}_i)\rangle_{\Gamma_{i,j}}\Big\} \\ &\quad + 2\,(B\boldsymbol{u},\boldsymbol{v})_{\tilde{K}} + \frac{1}{2}\langle (\mathsf{N} + D)\boldsymbol{u}, \boldsymbol{v}\rangle_{\Gamma_e(\tilde{K})}. \end{aligned}$$

Proof
We add (11) over the elements in $\tilde{K}$ to obtain

$$a_{\tilde{K}}(\boldsymbol{u},\boldsymbol{v}) = -\sum_{K\subset\tilde{K}} (\boldsymbol{u}, \mathcal{L}\boldsymbol{v})_K + 2\,(B\boldsymbol{u},\boldsymbol{v})_{\tilde{K}} + \langle \boldsymbol{u}, \mathcal{M}\boldsymbol{v}\rangle_{\Gamma_{\rm out}(\tilde{K})}$$

$$
\begin{aligned}
& -\langle \boldsymbol{u}_{\text{ext}}, \mathcal{M}\boldsymbol{v}\rangle_{\Gamma_{in}(\tilde{K})} + \frac{1}{2}\langle (\mathsf{N}+D)\boldsymbol{u}, \boldsymbol{v}\rangle_{\Gamma_e(\tilde{K})} \\
& + \sum_{\Gamma_{i,j}\in G(\tilde{K}), i<j} \Big\{ \langle \boldsymbol{u}_i, \mathsf{M}_i^+ \boldsymbol{v}_i\rangle_{\Gamma_{i,j}} + \langle \boldsymbol{u}_j, \mathsf{M}_i^- \boldsymbol{v}_i\rangle_{\Gamma_{i,j}} \\
& \qquad + \langle \boldsymbol{u}_j, \mathsf{M}_j^+ \boldsymbol{v}_j\rangle_{\Gamma_{i,j}} + \langle \boldsymbol{u}_i, \mathsf{M}_j^- \boldsymbol{v}_j\rangle_{\Gamma_{i,j}} \Big\} \\
= & -\sum_{K\subset\tilde{K}} (\boldsymbol{u}, \mathcal{L}\boldsymbol{v})_K + 2\,(B\boldsymbol{u}, \boldsymbol{v})_{\tilde{K}} + \langle \boldsymbol{u}, \mathcal{M}\boldsymbol{v}\rangle_{\Gamma_{\text{out}}(\tilde{K})} \\
& -\langle \boldsymbol{u}_{\text{ext}}, \mathcal{M}\boldsymbol{v}_{\text{ext}} + (\boldsymbol{v}-\boldsymbol{v}_{\text{ext}})\rangle_{\Gamma_{in}(\tilde{K})} + \frac{1}{2}\langle (\mathsf{N}+D)\boldsymbol{u}, \boldsymbol{v}\rangle_{\Gamma_e(\tilde{K})} \\
& + \sum_{\Gamma_{i,j}\in G(\tilde{K}), i<j} \Big\{ \langle \boldsymbol{u}_i, \mathsf{M}_i^+ \boldsymbol{v}_i\rangle_{\Gamma_{i,j}} + \langle \boldsymbol{u}_j, \mathsf{M}_i^- (\boldsymbol{v}_j + (\boldsymbol{v}_i - \boldsymbol{v}_j))\rangle_{\Gamma_{i,j}} \\
& \qquad + \langle \boldsymbol{u}_j, \mathsf{M}_j^+ \boldsymbol{v}_j\rangle_{\Gamma_{i,j}} + \langle \boldsymbol{u}_i, \mathsf{M}_j^- \boldsymbol{v}_i + (\boldsymbol{v}_j - \boldsymbol{v}_i)\rangle_{\Gamma_{i,j}} \Big\}
\end{aligned}
$$

Cancelling the obvious terms using (16)-(18) produces the desired result.

We can now prove the following basic existence and uniqueness result.

Lemma 4 *Under the assumptions on the data and mesh given in Section 2, there exists a unique discrete solution $\boldsymbol{u}_h$ to (14).*

Proof

Because of the explicit coupling among macroelements, we may show $\boldsymbol{u}_h$ is well-defined over Ω_T by showing it is well-defined over a single macroelement $\tilde{K}$. When applied over $K \subset \tilde{K}$, equations (14) can be formulated as a set of linear algebraic equations $A\hat{u} = b$ for a set of nodal values $\hat{u}$ defining $\boldsymbol{u}_h$ in $\tilde{K}$, and b depends on $\boldsymbol{f}$ in $\tilde{K}$, $\boldsymbol{g}$ on $\Gamma_e(\tilde{K})$, and $\boldsymbol{u}_{h,\text{ext}}$ on $\Gamma_{\text{in}}(\tilde{K})$. To show that $\hat{u}$ is well-defined, we show that this linear system has only the trivial solution $\hat{u} = 0$ if $b = 0$. This is equivalent to showing that if

$$
\begin{aligned}
a_K(\boldsymbol{u}_h, \boldsymbol{v}_h) &= 0 \quad \text{for all } \boldsymbol{v}_h \in (P_p(K))^m \text{ and } K \subset \tilde{K}, \\
\boldsymbol{u}_{h,\text{ext}} &= 0 \quad \text{on } \Gamma_{\text{in}}(\tilde{K}),
\end{aligned}
$$

then $\boldsymbol{u}_h \equiv 0$ in $\tilde{K}$.

Summing $a_K(\boldsymbol{u}_h, \boldsymbol{v}_h) = 0$ over $K \subset \tilde{K}$ and applying the result of Lemma 2 we obtain

$$
\begin{aligned}
& \langle \boldsymbol{u}_h, \mathcal{M}\boldsymbol{u}_h\rangle_{\Gamma_{\text{out}}(\tilde{K})} + \langle [\boldsymbol{u}_h], \mathcal{M}[\boldsymbol{u}_h]\rangle_{\Gamma_{\text{in}}(\tilde{K})\cup G(\tilde{K})} \\
& \qquad + 2\,(B\boldsymbol{u}_h, \boldsymbol{u}_h)_{\tilde{K}} + \langle \boldsymbol{u}_h, \mathcal{M}\boldsymbol{u}_h\rangle_{\Gamma_e(\tilde{K})} = 0.
\end{aligned}
$$

Since all the terms on the left hand side are nonnegative, we conclude that $\boldsymbol{u}_h = 0$ on $\Gamma_{\text{out}}(\tilde{K})$, $\mathcal{M}[\boldsymbol{u}_h] = 0$ on $\Gamma_{\text{in}}(\tilde{K})$ (implying $\boldsymbol{u}_h = 0$ on $\Gamma_{\text{in}}(\tilde{K})$), and $\mathcal{M}[\boldsymbol{u}_h] = 0$ on $G(\tilde{K})$. Also, under the assumption that B is symmetric we can see that $B\boldsymbol{u}_h = 0$. Hence $\mathcal{L}\boldsymbol{u}_h = A\boldsymbol{u}_{h,t} + \sum_{i=1}^N A_i \boldsymbol{u}_{h,x_i}$ and under the assumption that A is constant on K we conclude that $\mathcal{L}\boldsymbol{u}_h \in (P_{p-1}(K))^m$. Further, our control over $[\boldsymbol{u}_h]$ implies that for each $K \subset \tilde{K}$, $\mathsf{M}^-(\boldsymbol{u}_{h,\text{ext}} - \boldsymbol{u}_h) = 0$ on $\Gamma_i(K)$. From (12) we therefore obtain

$$
(\mathcal{L}\boldsymbol{u}_h, \boldsymbol{v}_h)_K + \frac{1}{2}\langle (\mathsf{N}-D)\boldsymbol{u}_h, \boldsymbol{v}_h\rangle_{\Gamma_e(K)} = 0 \quad \text{for all } \boldsymbol{v}_h \in (P_p(K))^m.
$$

By assumption, $\Gamma_e(K)$ consists of at most one face. Let f^* denote this face if $\Gamma_e(K) \neq \emptyset$, otherwise take f^* to be an arbitrary face of $\Gamma(K)$. Then define $\boldsymbol{w}_h \in (P_p(K))^m$ by

$$\begin{aligned} &\boldsymbol{w}_h = 0 && \text{on } f^*, \\ &(\boldsymbol{w}_h, \boldsymbol{\eta}_h)_K = (\mathcal{L}\boldsymbol{u}_h, \boldsymbol{\eta}_h)_K && \text{for all } \boldsymbol{\eta}_h \in (P_{p-1}(K))^m. \end{aligned}$$

It is easy to see that $\boldsymbol{w}_h$ is well-defined, and that it satisfies $(\mathcal{L}\boldsymbol{u}_h, \boldsymbol{w}_h)_K = \|\mathcal{L}\boldsymbol{u}_h\|_K^2$ (since $\mathcal{L}\boldsymbol{u}_h \in (P_{p-1}(K))^m$) and $\langle(\mathsf{N} - D)\boldsymbol{u}_h, \boldsymbol{w}_h\rangle_{\Gamma_e(K)} = 0$. By taking $\boldsymbol{v}_h = \boldsymbol{w}_h$ above, we thus conclude that $\mathcal{L}\boldsymbol{u}_h \equiv 0$ in K.

Now by assumption, for each simplex $K \subset \tilde{K}$, $\Gamma(K)$ has a nonempty intersection with $\Gamma_{\text{in}}(\tilde{K})$ or $\Gamma_{\text{out}}(\tilde{K})$. Assuming the former, it is always possible to construct a simplex $K' \subset K$ with one inflow face $f' \subset \Gamma_{\text{in}}(K) \cap \Gamma_{\text{in}}(\tilde{K})$ (where $\boldsymbol{u}_h = 0$) and all other faces outflow. We claim $\boldsymbol{u}_h$ vanishes identically on K'. For if there is a point $P \in K'$ such that $\boldsymbol{u}_h(P) \neq 0$, then f' and P define another simplex $K'' \subset K'$ with inflow face f' and all other faces outflow, and (see (10)):

$$0 = (\mathcal{L}\boldsymbol{u}_h, \boldsymbol{u}_h)_{K''} = \frac{1}{2}\langle \mathcal{M}\boldsymbol{u}_h, \boldsymbol{u}_h\rangle_{\Gamma_{\text{out}}(K'')}.$$

This implies $\boldsymbol{u}_h = 0$ along $\Gamma_{\text{out}}(K'')$, in particular at point P. Since $\boldsymbol{u}_h|_K$ is the extension of the polynomial $\boldsymbol{u}_h|_{K'}$ to all of K, we conclude that $\boldsymbol{u}_h$ vanishes identically in K.

As a footnote to the above proof, we infer that $\|\boldsymbol{u}_h\|_{\tilde{K}}$ can be bounded in terms of $|\boldsymbol{u}_{h,\text{ext}}|_{\Gamma_{\text{in}}(\tilde{K})}$, $\|\boldsymbol{f}\|_{\tilde{K}}$, and $|\boldsymbol{g}|_{\Gamma_e(\tilde{K}}$. Taking into account the proper scaling of these norms (which may be seen by a piecewise affine mapping of $\tilde{K}$ into a reference macroelement, as in Lemma 3.2 of [5]), we obtain

$$\|\boldsymbol{u}_h\|_{\tilde{K}} \leq C\left(\sqrt{h_{\tilde{K}}}(|\boldsymbol{u}_{h,\text{ext}}|_{\Gamma_{\text{in}}(\tilde{K})} + |\boldsymbol{g}|_{\Gamma_e(\tilde{K})}) + h_{\tilde{K}}\|\boldsymbol{f}\|_{\tilde{K}}\right) \tag{22}$$

where $h_{\tilde{K}} \equiv \max_{K \subset \tilde{K}} h_K$, and C is independent of $\tilde{K}$ and $\boldsymbol{u}_h$.

5 Error Estimates

In this section we prove the main theorem of this paper, an error estimate for our discontinuous Galerkin method. Let Ω_t denote a collection of macroelements $\{\tilde{K}\} \subset \tau_h$ such that $\Gamma_{\text{in}}(\Omega_t) \subset \Gamma_{\text{in}}(\Omega_T) = \Omega \times \{t = 0\}$. Thus $\boldsymbol{u}_h$ can be computed first in Ω_t, then in $\Omega_T \setminus \Omega_t$, without violating any domain of dependence requirements.

Theorem 1 *Suppose the solution $\boldsymbol{u}$ of the continuous problem (1)–(4) is such that $\boldsymbol{u}|_K \in (H^{p+1}(K))^m$ for all elements $K \in \tau_h$, that the discrete solution $\boldsymbol{u}_h$ of (14) is chosen to be the $L^2(\Omega)$ projection of the initial data, and that Ω_t is a space-time domain as described above. Then there is a constant C independent of t, τ_h, $\boldsymbol{u}$ and $\boldsymbol{u}_h$ such that*

$$|\boldsymbol{u} - \boldsymbol{u}_h|^2_{\Gamma_{\text{out}}(\Omega_t)} + \sum_{\tilde{K} \subset \Omega_t} \left\{ |[\boldsymbol{u} - \boldsymbol{u}_h]|^2_{\Gamma_{\text{in}}(\tilde{K})} + |\mathcal{M}^{1/2}[\boldsymbol{u} - \boldsymbol{u}_h]|^2_{G(\tilde{K})} \right\}$$

$$+\|B^{1/2}(\boldsymbol{u}-\boldsymbol{u}_h)\|^2_{\Omega_l}+|(\mathsf{N}+\mathsf{N}^T)^{1/2}(\boldsymbol{u}-\boldsymbol{u}_h)|^2_{\Gamma_e(\Omega_t)}$$
$$\leq C\sum_{K\in\Omega_t} h_K^{2p+1}\|\boldsymbol{u}\|^2_{p+1,K}. \tag{23}$$

Remarks. Of course the above estimate implies that if the true solution is smooth enough, the error bound is $O(h^{p+1/2})$. This is an optimal estimate for the error on surfaces in the mesh (e.g., on $\Gamma_{\rm out}(\Omega_t)$) but the interior estimate is non-optimal.

The choice of the projection as initial data for the discrete problem is not a computational challenge since it can be computed element by element. In fact we can also use the interpolant if the initial data is smooth enough.

If $\boldsymbol{u}$ has reduced regularity, we can obtain a lower order approximation using error estimates for the appropriate generalized interpolant used in the upcoming proof.

Proof

Subtracting (14) from (13), we get that $a_{\tilde{K}}(\boldsymbol{u}-\boldsymbol{u}_h,\boldsymbol{v}_h)=0$ for all $\boldsymbol{v}_h$ such that $\boldsymbol{v}_h|_K\in(P_p(K))^m$ for each element $K\subset\tilde{K}$. Let $\boldsymbol{w}_h$ be any piecewise polynomial such that $\boldsymbol{w}_h|_K\in(P_p(K))^m$ for each K (we shall shortly say how to choose $\boldsymbol{w}_h$) and let $\boldsymbol{e}_h=\boldsymbol{w}_h-\boldsymbol{u}_h$. Then

$$a_{\tilde{K}}(\boldsymbol{e}_h,\boldsymbol{v}_h)=a_{\tilde{K}}(\boldsymbol{w}_h-\boldsymbol{u},\boldsymbol{v}_h) \tag{24}$$

for all $\boldsymbol{v}_h$ such that $\boldsymbol{v}_h|_K\in(P_p(K))^m$. In particular,

$$a_{\tilde{K}}(\boldsymbol{e}_h,\boldsymbol{e}_h)=a_{\tilde{K}}(\boldsymbol{w}_h-\boldsymbol{u},\boldsymbol{e}_h).$$

Using the conclusion of Lemmas 2 and 3,

$$\begin{aligned}
&\frac{1}{2}\Big\{\langle\boldsymbol{e}_h,\mathcal{M}\boldsymbol{e}_h\rangle_{\Gamma_{\rm out}(\tilde{K})}-\langle\boldsymbol{e}_{h,\rm ext},\mathcal{M}\boldsymbol{e}_{h,\rm ext}\rangle_{\Gamma_{\rm in}(\tilde{K})}+\langle[\boldsymbol{e}_h],\mathcal{M}[\boldsymbol{e}_h]\rangle_{\Gamma_{\rm in}(\tilde{K})\cup G(\tilde{K})}\Big\}\\
&\qquad\qquad +(\mathcal{B}\boldsymbol{e}_h,\boldsymbol{e}_h)_{\tilde{K}}+\frac{1}{2}\langle\boldsymbol{e}_h,\mathsf{N}\boldsymbol{e}_h\rangle_{\Gamma_e(\tilde{K})}\\
=\;&-\sum_{K\subset\tilde{K}}(\boldsymbol{w}_h-\boldsymbol{u},\mathcal{L}\boldsymbol{e}_h)_K+\langle\boldsymbol{w}_h-\boldsymbol{u},\mathcal{M}\boldsymbol{e}_h\rangle_{\Gamma_{\rm out}(\tilde{K})}\\
&-\langle(\boldsymbol{w}_h-\boldsymbol{u})_{\rm ext},\mathcal{M}\boldsymbol{e}_{h,\rm ext}\rangle_{\Gamma_{\rm in}(\tilde{K})}+\langle(\boldsymbol{w}_h-\boldsymbol{u})_{\rm ext},\mathcal{M}[\boldsymbol{e}_h]\rangle_{\Gamma_{\rm in}(\tilde{K})}\\
&+\sum_{\Gamma_{i,j}\in G(\tilde{K}),\ i<j}\Big\{\langle(\boldsymbol{w}_h-\boldsymbol{u})_j,\mathsf{M}_i^-((\boldsymbol{e}_h)_i-(\boldsymbol{e}_h)_j)\rangle_{\Gamma_{i,j}}\\
&\qquad\qquad +\langle(\boldsymbol{w}_h-\boldsymbol{u})_i,\mathsf{M}_j^-((\boldsymbol{e}_h)_j-(\boldsymbol{e}_h)_i)\rangle_{\Gamma_{i,j}}\Big\}\\
&+2(B(\boldsymbol{w}_h-\boldsymbol{u}),\boldsymbol{e}_h)_{\tilde{K}}+\frac{1}{2}\langle(\mathsf{N}+D)(\boldsymbol{w}_h-\boldsymbol{u}),\boldsymbol{e}_h\rangle_{\Gamma_e(\tilde{K})}.
\end{aligned}\tag{25}$$

We can immediately simplify this expression by making a suitable choice of the function $\boldsymbol{w}_h$. If $\Gamma_e(K)\neq\emptyset$, we let $f^*=\Gamma_e(K)$ (recall we have assumed that each element meets the boundary on at most one face). Otherwise we just

select f^* to be some face on $\Gamma_{\text{in}}(K)$. Then, on K, we define $\boldsymbol{w}_h \in (P_p(K))^m$ by requiring that

$$\int_K (\boldsymbol{u} - \boldsymbol{w}_h) \cdot \boldsymbol{\phi}_h \, dV = 0 \quad \text{for all } \boldsymbol{\phi}_h \in (P_{p-1}(K))^m, \tag{26}$$

$$\int_{f^*} (\boldsymbol{u} - \boldsymbol{w}_h) \cdot \boldsymbol{\phi}_h \, dA = 0 \quad \text{for all } \boldsymbol{\phi}_h \in (P_p(f^*))^m. \tag{27}$$

This is the same definition as used in [5] and hence $\boldsymbol{w}_h$ is an optimal order generalized interpolant. Since we have assumed that the matrices A and A_j, $j = 1, ..., N$ are constant on each element, and since B is assumed to be symmetric, we have

$$\begin{aligned} &- \sum_{K \subset \tilde{K}} (\boldsymbol{w}_h - \boldsymbol{u}, \mathcal{L}\boldsymbol{e}_h)_K + (B(\boldsymbol{w}_h - \boldsymbol{u}), \boldsymbol{e}_h)_{\tilde{K}} \\ &\qquad = - \sum_{K \subset \tilde{K}} \left(\boldsymbol{w}_h - \boldsymbol{u}, A\boldsymbol{e}_{h,t} + \sum_{j=1}^{N} A_j \boldsymbol{e}_{h,x_j} \right)_K = 0, \end{aligned}$$

where the last equality follows from (26). Using (27) and the face that D and N are constant on each face we have

$$\frac{1}{2} \langle (\mathsf{N} + D)(\boldsymbol{w}_h - \boldsymbol{u}), \boldsymbol{e}_h \rangle_{\Gamma_e(\tilde{K})} = 0.$$

Furthermore, completing the square, and defining $\boldsymbol{e} = \boldsymbol{u} - \boldsymbol{u}_h$, we obtain

$$\begin{aligned} \frac{1}{2} \langle \boldsymbol{e}_h, \mathcal{M}\boldsymbol{e}_h \rangle_{\Gamma_{\text{out}}(\tilde{K})} &- \langle \boldsymbol{w}_h - \boldsymbol{u}, \mathcal{M}\boldsymbol{e}_h \rangle_{\Gamma_{\text{out}}(\tilde{K})} \\ &= \frac{1}{2} \langle \boldsymbol{e}, \mathcal{M}\boldsymbol{e} \rangle_{\Gamma_{\text{out}}(\tilde{K})} - \frac{1}{2} \langle \boldsymbol{w}_h - \boldsymbol{u}, \mathcal{M}(\boldsymbol{w}_h - \boldsymbol{u}) \rangle_{\Gamma_{\text{out}}(\tilde{K})}. \end{aligned}$$

In the same way

$$\begin{aligned} &-\frac{1}{2} \langle \boldsymbol{e}_{h,\text{ext}}, \mathcal{M}\boldsymbol{e}_{h,\text{ext}} \rangle_{\Gamma_{\text{in}}(\tilde{K})} + \langle (\boldsymbol{w}_h - \boldsymbol{u})_{\text{ext}}, \mathcal{M}\boldsymbol{e}_{h,\text{ext}} \rangle_{\Gamma_{\text{in}}(\tilde{K})} \\ = \; &-\frac{1}{2} \langle \boldsymbol{e}_{\text{ext}}, \mathcal{M}\boldsymbol{e}_{\text{ext}} \rangle_{\Gamma_{\text{in}}(\tilde{K})} + \frac{1}{2} \langle (\boldsymbol{w}_h - \boldsymbol{u})_{\text{ext}}, \mathcal{M}(\boldsymbol{w}_h - \boldsymbol{u})_{\text{ext}} \rangle_{\Gamma_{\text{in}}(\tilde{K})}. \end{aligned}$$

Using these results (25) becomes

$$\begin{aligned} &\frac{1}{2} \left\{ \langle \boldsymbol{e}, \mathcal{M}\boldsymbol{e} \rangle_{\Gamma_{\text{out}}(\tilde{K})} - \langle \boldsymbol{e}_{\text{ext}}, \mathcal{M}\boldsymbol{e}_{\text{ext}} \rangle_{\Gamma_{\text{in}}(\tilde{K})} + \langle [\boldsymbol{e}_h], \mathcal{M}[\boldsymbol{e}_h] \rangle_{\Gamma_{\text{in}}(\tilde{K}) \cup G(\tilde{K})} \right\} \\ &\qquad + (B\boldsymbol{e}_h, \boldsymbol{e}_h)_{\tilde{K}} + \frac{1}{2} \langle \boldsymbol{e}_h, \mathsf{N}\boldsymbol{e}_h \rangle_{\Gamma_e(\tilde{K})} \\ = \; &\frac{1}{2} \langle \boldsymbol{w}_h - \boldsymbol{u}, \mathcal{M}(\boldsymbol{w}_h - \boldsymbol{u}) \rangle_{\Gamma_{\text{out}}(\tilde{K})} - \frac{1}{2} \langle (\boldsymbol{w}_h - \boldsymbol{u})_{\text{ext}}, \mathcal{M}(\boldsymbol{w}_h - \boldsymbol{u})_{\text{ext}} \rangle_{\Gamma_{\text{in}}(\tilde{K})} \\ &+ \langle (\boldsymbol{w}_h - \boldsymbol{u})_{\text{ext}}, \mathcal{M}[\boldsymbol{e}_h] \rangle_{\Gamma_{in}(\tilde{K})} \\ &+ \sum_{\Gamma_{i,j} \in G(\tilde{K}),\, i<j} \left\{ \langle (\boldsymbol{w}_h - \boldsymbol{u})_j, \mathsf{M}_i^-((\boldsymbol{e}_h)_i - (\boldsymbol{e}_h)_j) \rangle_{\Gamma_{i,j}} \right. \\ &\qquad \left. + \langle (\boldsymbol{w}_h - \boldsymbol{u})_i, \mathsf{M}_j^-((\boldsymbol{e}_h)_j - (\boldsymbol{e}_h)_i) \rangle_{\Gamma_{i,j}} \right\} \\ &+ (B(\boldsymbol{w}_h - \boldsymbol{u}), \boldsymbol{e}_h)_{\tilde{K}}. \end{aligned} \tag{28}$$

Now suppose Ω_t is a space-time domain as described before Theorem 1. Adding the above estimate we obtain

$$\begin{aligned}
&\frac{1}{2}\left\{\langle \boldsymbol{e},\mathcal{M}\boldsymbol{e}\rangle_{\Gamma_{\rm out}(\Omega_t)}-\langle \boldsymbol{e}_{\rm ext},\mathcal{M}\boldsymbol{e}_{\rm ext}\rangle_{\Gamma_{\rm in}(\Omega_t)}+\sum_{\tilde{K}\subset\Omega_t}\langle[\boldsymbol{e}_h],\mathcal{M}[\boldsymbol{e}_h]\rangle_{\Gamma_{\rm in}(\tilde{K})\cup G(\tilde{K})}\right\}\\
&\qquad\qquad +(B\boldsymbol{e}_h,\boldsymbol{e}_h)_{\Omega_t}+\frac{1}{2}\langle \boldsymbol{e}_h,\mathsf{N}\boldsymbol{e}_h\rangle_{\Gamma_e(\Omega_t)}\\
=\;&\frac{1}{2}\langle \boldsymbol{w}_h-\boldsymbol{u},\mathcal{M}(\boldsymbol{w}_h-\boldsymbol{u})\rangle_{\Gamma_{\rm out}(\Omega_t)}-\frac{1}{2}\langle(\boldsymbol{w}_h-\boldsymbol{u})_{\rm ext},\mathcal{M}(\boldsymbol{w}_h-\boldsymbol{u})_{\rm ext}\rangle_{\Gamma_{\rm in}(\Omega_t)}\\
&+\sum_{\tilde{K}\subset\Omega_t}\left\{\langle(\boldsymbol{w}_h-\boldsymbol{u})_{\rm ext},\mathcal{M}[\boldsymbol{e}_h]\rangle_{\Gamma_{\rm in}(\tilde{K})}\right.\\
&\qquad+\sum_{\Gamma_{i,j}\in G(\tilde{K}),\ i<j}\big\{\langle(\boldsymbol{w}_h-\boldsymbol{u})_j,\mathsf{M}_i^-((\boldsymbol{e}_h)_i-(\boldsymbol{e}_h)_j)\rangle_{\Gamma_{i,j}}\\
&\qquad\qquad\left.+\langle(\boldsymbol{w}_h-\boldsymbol{u})_i,\mathsf{M}_j^-((\boldsymbol{e}_h)_j-(\boldsymbol{e}_h)_i)\rangle_{\Gamma_{i,j}}\big\}\right\}\\
&+(B(\boldsymbol{w}_h-\boldsymbol{u}),\boldsymbol{e}_h)_{\Omega_t}. \qquad (29)
\end{aligned}$$

Using the Cauchy-Schwarz and arithmetic geometric mean inequality, we see that for any $\epsilon>0$

$$\begin{aligned}
&\frac{1}{2}\left\{\langle \boldsymbol{e},\mathcal{M}\boldsymbol{e}\rangle_{\Gamma_{\rm out}(\Omega_t)}-\langle \boldsymbol{e}_{\rm ext},\mathcal{M}\boldsymbol{e}_{\rm ext}\rangle_{\Gamma_{\rm in}(\Omega_t)}+\sum_{\tilde{K}\subset\Omega_t}\langle[\boldsymbol{e}_h],\mathcal{M}[\boldsymbol{e}_h]\rangle_{\Gamma_{\rm in}(\tilde{K})\cup G(\tilde{K})}\right\}\\
&\qquad\qquad +(B\boldsymbol{e}_h,\boldsymbol{e}_h)_{\Omega_t}+\frac{1}{2}\langle \boldsymbol{e}_h,\mathsf{N}\boldsymbol{e}_h\rangle_{\Gamma_e(\Omega_t)}\\
\le\;&\frac{1}{2}|\mathcal{M}^{1/2}(\boldsymbol{w}_h-\boldsymbol{u})|^2_{\Gamma_{\rm out}(\Omega_t)}-\frac{1}{2}|\mathcal{M}^{1/2}(\boldsymbol{w}_h-\boldsymbol{u})_{\rm ext}|^2_{\Gamma_{\rm in}(\Omega_t)}\\
&+\sum_{\tilde{K}\subset\Omega_t}\left\{\frac{1}{2\epsilon}|\mathcal{M}^{1/2}(\boldsymbol{w}_h-\boldsymbol{u})_{\rm ext}|^2_{\Gamma_{\rm in}(\tilde{K})}+\frac{\epsilon}{2}|\mathcal{M}^{1/2}[\boldsymbol{e}_h]|^2_{\Gamma_{\rm in}(\tilde{K})}\right.\\
&\qquad+\sum_{\Gamma_{i,j}\in G(\tilde{K}),\ i<j}\left\{\frac{1}{2\epsilon}|(-\mathsf{M}_i^-)^{1/2}(\boldsymbol{w}_h-\boldsymbol{u})_j|^2_{\Gamma_{i,j}}+\frac{\epsilon}{2}|(-\mathsf{M}_i^-)^{1/2}[\boldsymbol{e}_h]|^2_{\Gamma_{i,j}}\right.\\
&\qquad\qquad\left.\left.+\frac{1}{2\epsilon}|(-\mathsf{M}_j^-)^{1/2}(\boldsymbol{w}_h-\boldsymbol{u})_i|^2_{\Gamma_{i,j}}+\frac{\epsilon}{2}|(-\mathsf{M}_j^-)^{1/2}[\boldsymbol{e}_h]|^2_{\Gamma_{i,j}}\right\}\right\}\\
&+\frac{1}{2\epsilon}\|B^{1/2}(\boldsymbol{w}_h-\boldsymbol{u})\|^2_{\Omega_t}+\frac{\epsilon}{2}\|B^{1/2}\boldsymbol{e}_h\|^2_{\Omega_t}. \qquad (30)
\end{aligned}$$

Choosing $\epsilon=1/2$ we obtain

$$\begin{aligned}
&\frac{1}{2}\langle \boldsymbol{e},\mathcal{M}\boldsymbol{e}\rangle_{\Gamma_{\rm out}(\Omega_t)}+\frac{1}{4}\sum_{\tilde{K}\subset\Omega_t}\langle[\boldsymbol{e}_h],\mathcal{M}[\boldsymbol{e}_h]\rangle_{\Gamma_{\rm in}(\tilde{K})\cup G(\tilde{K})}\\
&\qquad\qquad+\frac{3}{4}\|B^{1/2}\boldsymbol{e}_h\|^2_{\Omega_t}+\frac{1}{2}\langle \boldsymbol{e}_h,\mathsf{N}\boldsymbol{e}_h\rangle_{\Gamma_e(\Omega_t)}\\
\le\;&\frac{1}{2}\langle \boldsymbol{e}_{\rm ext},\mathcal{M}\boldsymbol{e}_{\rm ext}\rangle_{\Gamma_{\rm in}(\Omega_t)}+\frac{1}{2}|\mathcal{M}^{1/2}(\boldsymbol{w}_h-\boldsymbol{u})|^2_{\Gamma_{\rm out}(\Omega_t)}
\end{aligned}$$

$$-\frac{1}{2}|\mathcal{M}^{1/2}(\boldsymbol{w}_h-\boldsymbol{u})_{\rm ext}|^2_{\Gamma_{\rm in}(\Omega_l)}+\sum_{\tilde{K}\subset\Omega_t}\left\{|\mathcal{M}^{1/2}(\boldsymbol{w}_h-\boldsymbol{u})_{\rm ext}|^2_{\Gamma_{\rm in}(\tilde{K})}\right.$$

$$\left.+\sum_{\Gamma_{i,j}\in G(\tilde{K})i<j}\left\{|(-\mathsf{M}_i^-)^{1/2}(\boldsymbol{w}_h-\boldsymbol{u})_j|^2_{\Gamma_{i,j}}+|(-\mathsf{M}_j^-)^{1/2}(\boldsymbol{w}_h-\boldsymbol{u})_i|^2_{\Gamma_{i,j}}\right\}\right\}$$

$$+\|B^{1/2}(\boldsymbol{w}_h-\boldsymbol{u})\|^2_{\Omega_t}. \tag{31}$$

Now the error in $\boldsymbol{w}_h$ satisfies the estimate

$$\|\boldsymbol{w}_h-\boldsymbol{u}\|^2_K+h_K|\boldsymbol{w}_h-\boldsymbol{u}|^2_{\Gamma(K)}\le Ch_K^{2p+2}\|\boldsymbol{u}\|^2_{p+1,K}, \tag{32}$$

where the constant C is independent of K, τ_h, and $\boldsymbol{u}$. Therefore, if the solution $\boldsymbol{u}$ is sufficiently regular and the discrete initial data is chosen as the $L^2(\Omega)$ projection of the true initial data, we obtain a bound $C\sum_{K\subset\Omega_t}h_K^{2p+1}\|\boldsymbol{u}\|^2_{p+1,K}$ for the right hand side of (31). The desired result now follows using the triangle inequality and the equivalence of unweighted and $\mathcal{M}$-weighted L^2 norms on inflow and outflow boundaries.

We now focus on obtaining an interior error estimate for $\boldsymbol{u}_h$. Toward this end, we partition the macroelements in τ_h into "layers" $L_1,...,L_m$ and subdomains $\Omega_i\equiv\cup_{j\le i}L_j$ subject to the following conditions:

- $\Gamma_{\rm in}(L_i)\subset\Gamma_{\rm in}(\Omega_T)\cup\Gamma_{\rm out}(\Omega_{i-1})$
- $\Gamma_{\rm in}(\tilde{K})\cap\Gamma_{\rm in}(\tilde{K}')=\emptyset$ for all macroelements $\tilde{K},\tilde{K}'\subset L_i$.

In other words, we may first compute $\boldsymbol{u}_h$, in parallel, in the macroelements comprising L_1, then in L_2, etc. The trivial option of choosing layers to be individual macroelements is of no interest to us. In fact, the usefulness of the concept derives from the possibility of choosing layers consisting of large numbers of macroelements, indicative of a high degree of parallelism in the coupling among elements.

Theorem 2 *Suppose that $\Omega_T=\cup_{i=1}^m L_i$ where the layers L_i are as described above, that $h_i\equiv\max_{K\subset L_i}h_K$ is the "width" of layer L_i, and that the conditions of Theorem 1 hold. Then there is a constant C independent of $\boldsymbol{u}$, $\boldsymbol{u}_h$, and τ_h such that*

$$\|\boldsymbol{u}-\boldsymbol{u}_h\|^2_{\Omega_T}\le C\left(\sum_{i=1}^m h_i\right)\sum_{K\subset\Omega_T}h_K^{2p+1}\|\boldsymbol{u}\|^2_{p+1,K}.$$

Remarks. If the tent-pitching algorithm is applied over Ω_T starting from a quasi-uniform spatial mesh of size h at $t=0$, the resulting space-time mesh will be quasi-uniform of size h and have $m=O(h^{-1})$ layers of width h. Then $\sum_{i=1}^m h_i$ will be uniformly bounded, and we get an estimate $\|\boldsymbol{u}-\boldsymbol{u}_h\|_{\Omega_T}\le O(h^{p+1/2})$ for $\boldsymbol{u}_h$, which, though suboptimal, is typical for discontinuous Galerkin methods. As we shall see shortly, numerical results suggest that an optimal convergence rate is seen in practice for uniform grids. It is also possible to achieve a uniformly bounded sum $\sum_{i=1}^m h_i$ for certain piecewise

quasi-uniform mesh refinement schemes, though here too we would expect the resulting $O(\sqrt{\sum_{K\subset\Omega_T} h_K^{2p+1}\|\boldsymbol{u}_h\|_{p+1,K}^2})$ estimate for $\boldsymbol{u}_h$ to be overly conservative.

Proof: For $\boldsymbol{u}_h$ satisfying (14) we have the bound (22) for $\|\boldsymbol{u}_h\|_{\tilde{K}}$. Analogously, using (24) we have

$$\|\boldsymbol{e}_h\|_{\tilde{K}}^2 \leq C\left(h_{\tilde{K}}|\boldsymbol{e}_{h,\mathrm{ext}}|_{\Gamma_{\mathrm{in}}(\tilde{K})}^2 + h_{\tilde{K}}^2\gamma_{\tilde{K}}^2\right)$$

where $\gamma_{\tilde{K}}$ satisfies

$$|a_{\tilde{K}}(\boldsymbol{w}_h - \boldsymbol{u}, \boldsymbol{v}_h)| \leq \gamma_{\tilde{K}}\|\boldsymbol{v}_h\|_{\tilde{K}}.$$

From (12) we get

$$\begin{aligned} a_{\tilde{K}}(\boldsymbol{w}_h - \boldsymbol{u}, \boldsymbol{v}_h) &\leq C\sum_{K\subset\tilde{K}}\big(\|\boldsymbol{w}_h - \boldsymbol{u}\|_{1,K}\cdot\|\boldsymbol{v}_h\|_K + |\boldsymbol{w}_h - \boldsymbol{u}|_{\Gamma(K)}\cdot|\boldsymbol{v}_h|_{\Gamma(K)} \\ &\qquad + |\mathsf{M}^-(\boldsymbol{w}_h - \boldsymbol{u})_{\mathrm{ext}}|_{\Gamma_i(K)}\cdot|\boldsymbol{v}_h|_{\Gamma_i(K)}\big) \\ &\leq C\sum_{K\subset\tilde{K}}\left(h_K^p\|\boldsymbol{u}\|_{p+1,K} + h_K^{-1/2}|\mathsf{M}^-(\boldsymbol{w}_h - \boldsymbol{u})_{\mathrm{ext}}|_{\Gamma_i(K)}\right)\cdot\|\boldsymbol{v}_h\|_{\tilde{K}}, \end{aligned}$$

where we have used (32) and the inverse inequality $|\boldsymbol{v}_h|_{\Gamma(T)} \leq Ch_K^{-1/2}\|\boldsymbol{v}_h\|_K$. Thus

$$\begin{aligned} \|\boldsymbol{e}_h\|_{\tilde{K}}^2 &\leq C\Bigg(h_{\tilde{K}}|\boldsymbol{e}_{h,\mathrm{ext}}|_{\Gamma_{\mathrm{in}}(\tilde{K})}^2 \\ &\qquad + \sum_{K\subset\tilde{K}}\left(h_K^{2p+2}\|\boldsymbol{u}_h\|_{p+1,K}^2 + h_K|\mathsf{M}^-(\boldsymbol{w}_h - \boldsymbol{u})_{\mathrm{ext}}|_{\Gamma_i(K)}^2\right)\Bigg). \quad (33) \end{aligned}$$

Summing (33) first over $\tilde{K}\subset L_i$, then over $i\in\{1,...,m\}$, and using (32) again, we get

$$\begin{aligned} \|\boldsymbol{e}_h\|_{L_i}^2 &\leq C\Bigg(h_i|\boldsymbol{e}_{h,\mathrm{cxt}}|_{\Gamma_{\mathrm{in}}(L_i)}^2 \\ &\qquad + \sum_{K\subset L_i}\left(h_K^{2p+2}\|\boldsymbol{u}_h\|_{p+1,K}^2 + h_K|\mathsf{M}^-(\boldsymbol{w}_h - \boldsymbol{u})_{\mathrm{ext}}|_{\Gamma_i(K)}^2\right)\Bigg), \end{aligned}$$

then

$$\|\boldsymbol{e}_h\|_{\Omega_T}^2 \leq C\left(\sum_{i=1}^m h_i|\boldsymbol{e}_{h,\mathrm{ext}}|_{\Gamma_{\mathrm{in}}(L_i)}^2 + \sum_{K\subset\Omega_T} h_K^{2p+2}\|\boldsymbol{u}\|_{p+1,K}^2\right).$$

Application of the triangle inequality inequality and (32) then gives

$$\|\boldsymbol{u} - \boldsymbol{u}_h\|_{\Omega_T}^2 \leq C\left(\sum_{i=1}^m h_i|\boldsymbol{u} - \boldsymbol{u}_{h,\mathrm{ext}}|_{\Gamma_{\mathrm{in}}(L_i)}^2 + \sum_{K\subset\Omega_T} h_K^{2p+2}\|\boldsymbol{u}\|_{p+1,K}^2\right). \quad (34)$$

Now $\Gamma_{\mathrm{in}}(L_i)\subset\Gamma_{\mathrm{in}}(\Omega_T)\cup\Gamma_{\mathrm{out}}(\Omega_{i-1})$, so via Theorem 1:

$$|\boldsymbol{u} - \boldsymbol{u}_{h,\mathrm{ext}}|_{\Gamma_{\mathrm{in}}(L_i)}^2 \leq C\sum_{K\subset\Omega_{i-1}} h_K^{2p+1}\|\boldsymbol{u}\|_{p+1,K}^2 \leq C\sum_{K\subset\Omega_T} h_K^{2p+1}\|\boldsymbol{u}\|_{p+1,K}^2.$$

Substituting into (34), we get the desired bound directly.

6 Acoustic wave equation

Our computational results to be presented in Section 7 are for the acoustic wave equation in $\mathbb{R}^2$. We next show how to write, in a standard way, this equation as a symmetric system. More interestingly, we show how to construct a family of matrices N that includes the usual Dirichlet and Neumann boundary conditions as well as the impedance boundary condition (often used as an absorbing boundary condition). The extension to 3D is obvious.

Let $\alpha, \beta \in L^\infty(\Omega)$ be bounded (almost everywhere) functions such that $\alpha \geq \alpha_0 > 0$ almost everywhere in Ω where α_0 is a constant, and $\beta \geq 0$. Then let γ denote a 2×2 symmetric matrix function of position such that $\gamma \in (L^\infty(\Omega))^{2\times 2}$ is bounded and uniformly positive definite on Ω (we also assume that α and γ are piecewise constant with respect to a polyhedral mesh of Ω). Then we seek to approximate the function u that satisfies

$$\alpha u_{tt} + \beta u_t = \nabla \cdot \left(\gamma^{-1} \nabla u\right) \qquad \text{in } \Omega,$$

subject to suitable boundary conditions which we shall detail shortly. This equation may be translated into the symmetric hyperbolic formulation as follows. Let the vector variable $\boldsymbol{u}$ be defined by

$$\boldsymbol{u} = \begin{pmatrix} u_t \\ \gamma^{-1}\nabla u \end{pmatrix}.$$

Then we see that the components of $\boldsymbol{u}$ satisfy

$$\begin{aligned} \alpha u_{1,t} + \beta u_1 &= \nabla \cdot \begin{pmatrix} u_2 \\ u_3 \end{pmatrix}, \\ \gamma \frac{\partial}{\partial t} \begin{pmatrix} u_2 \\ u_3 \end{pmatrix} &= \nabla u_1. \end{aligned}$$

These equations can be written as a symmetric hyperbolic system by writing

$$A = \left(\begin{array}{c|c} \alpha & 0 \\ \hline 0 & \gamma \end{array}\right), \quad B = \begin{pmatrix} \beta & 0 & 0 \\ 0 & 0 & 0 \\ 0 & 0 & 0 \end{pmatrix}, \tag{35}$$

and

$$A_1 = \begin{pmatrix} 0 & -1 & 0 \\ -1 & 0 & 0 \\ 0 & 0 & 0 \end{pmatrix}, \quad A_2 = \begin{pmatrix} 0 & 0 & -1 \\ 0 & 0 & 0 \\ -1 & 0 & 0 \end{pmatrix}.$$

Then the boundary matrix D is

$$D = \begin{pmatrix} 0 & -n_1 & -n_2 \\ -n_1 & 0 & 0 \\ -n_2 & 0 & 0 \end{pmatrix}. \tag{36}$$

This has eigenvalues $\lambda_1 = 1$, $\lambda_2 = 0$ and $\lambda_3 = -1$. Computing the eigenvectors and using the fact that $|\boldsymbol{n}| = 1$ we have

$$D^+ = \frac{1}{2} \begin{pmatrix} -1 \\ n_1 \\ n_2 \end{pmatrix} (-1, n_1, n_2),$$

$$D^- = -\frac{1}{2}\begin{pmatrix} 1 \\ n_1 \\ n_2 \end{pmatrix}(1, n_1, n_2),$$

and then $D = D^+ + D^-$, D^+ is positive semi-definite and D^- is negative semi-definite. In order to allow more general boundary conditions, it proves useful to generalize D^+ and D^- slightly. Note that if

$$S = \begin{pmatrix} \sigma & 0 & 0 \\ 0 & 1 & 0 \\ 0 & 0 & 1 \end{pmatrix}$$

and if $\sigma > 0$, then $\frac{1}{\sigma}SDS = D$ so that $D = \frac{1}{\sigma}SD^+S + \frac{1}{\sigma}SD^-S$ and the matrices $D_\sigma^+ = \frac{1}{\sigma}SD^+S$ and $D_\sigma^- = \frac{1}{\sigma}SD^-S$ are also a valid splitting of D (since the above is not a similarity transformation, this claim has to be checked as follows). Direct calculation shows that

$$D_\sigma^+ = \frac{1}{2\sigma}\begin{pmatrix} -\sigma \\ n_1 \\ n_2 \end{pmatrix}(-\sigma, n_1, n_2),$$

$$D_\sigma^- = -\frac{1}{2\sigma}\begin{pmatrix} \sigma \\ n_1 \\ n_2 \end{pmatrix}(\sigma, n_1, n_2),$$

and $D = D_\sigma^+ + D_\sigma^-$. The null-space condition is satisfied and the definiteness of the splitting is maintained if σ is strictly positive. In fact the non-zero eigenvalue of D_σ^+ is $(\sigma^2+1)/(2\sigma)$ and of D_σ^- is $-(\sigma^2+1)/(2\sigma)$. We can then define the following matrices

$$L^+ = \frac{1}{\sqrt{2\sigma}}(-\sigma, n_1, n_2) \quad \text{and} \quad L^- = \frac{1}{\sqrt{2\sigma}}(\sigma, n_1, n_2)$$

so that $D_\sigma^+ = (L^+)^T L^+$ and $D_\sigma^- = -(L^-)^T L^-$.

Given a function $g \in L^2(\Gamma)$ we would like to implement the impedance type boundary condition

$$\sigma u_t + \boldsymbol{n}_x \cdot (\gamma^{-1}\nabla u) = Q(-\sigma u_t + \boldsymbol{n}_x \cdot (\gamma^{-1}\nabla u)) + \sqrt{2\sigma}g. \tag{37}$$

This class of boundary conditions is fairly general. With the choice $Q = -1$ we obtain the Neumann boundary condition

$$\boldsymbol{n}_x \cdot (\gamma^{-1}\nabla u) = \frac{1}{\sqrt{2}}\sigma^{1/2}g$$

while with the choice $Q = 1$ we obtain the condition that

$$u_t = \frac{1}{\sqrt{2\sigma}}g$$

which is essentially a Dirichlet boundary condition. When $Q = 0$ we obtain the classical impedance boundary condition

$$\sigma u_t + \boldsymbol{n}_x \cdot (\gamma^{-1}\nabla u) = \sqrt{2\sigma}g.$$

For an appropriate choice of σ depending on the wave speed in the medium adjacent to the boundary, this is the lowest order Engquist-Majda absorbing boundary condition [3].

Using the definition of $\boldsymbol{u}$ and the matrices L^+ and L^- we see that (37) can be written

$$L^-\boldsymbol{u} = QL^+\boldsymbol{u} + g$$

and hence $(L^-)^T L^-\boldsymbol{u} = Q(L^-)^T L^+\boldsymbol{u} + (L^-)^T g$. We choose

$$\mathsf{N} = D - 2(D_\sigma^- + Q(L^-)^T L^+), \tag{38}$$

so that $(D - \mathsf{N})\boldsymbol{u} = 2(D_\sigma^- + Q(L^-)^T L^+)\boldsymbol{u} = -2(L^-)^T g$. Thus we choose the vector data for the symmetric system to be $\boldsymbol{g} = -2(L^-)^T g$.

Using (38), the eigenvalues of $\mathsf{N} + \mathsf{N}^T$ are $(0, 0, 2\sigma(Q+1), 2(1-Q)/\sigma)$ so $\mathsf{N} + \mathsf{N}^T$ is positive semidefinite if $|Q| \leq 1$ which is sufficient to include the standard boundary conditions and in this case (5) is satisfied. In addition (when $n_1 \neq 0$)

$$\ker(D + \mathsf{N}) = \text{span}\left\{ \begin{pmatrix} n_1 \\ \sigma \\ 0 \end{pmatrix}, \begin{pmatrix} 0 \\ -n_2 \\ n_1 \end{pmatrix} \right\},$$

$$\ker(D - \mathsf{N}) = \text{span}\left\{ \begin{pmatrix} 0 \\ -n_2 \\ n_1 \end{pmatrix}, \begin{pmatrix} n_1(Q-1) \\ \sigma(1+Q) \\ 0 \end{pmatrix} \right\},$$

so that in this case the kernel condition (6) is also satisfied. The kernel condition can also be checked when $n_1 = 0$.

Note that when $Q = 1$ and $\sigma = 1$ the choice of N in (38) reduces to the one used by Falk and Richter for the Dirichlet boundary condition:

$$\mathsf{N} = \begin{pmatrix} 2 & -n_1 & -n_2 \\ n_1 & 0 & 0 \\ n_2 & 0 & 0 \end{pmatrix}.$$

7 Numerical results in two dimensions

For this paper our numerical experiments are confined to two space dimensions (we hope to move to three space dimensions shortly). Since Maxwell's equations and the wave equation are identical in two dimensions, our examples are for the wave equation. In all the tests we take $\sigma = 1$.

7.1 Wave propagation

The first example is a simple verification of the order of convergence of the scheme in the case of vanishing initial data (the example is, having rescaled time, from Section 5.1 of [12]). The domain is $\Omega = [0, 2]^2$. The exact solution is

$$\boldsymbol{u} = \begin{pmatrix} f(t - \boldsymbol{k}\cdot\boldsymbol{x}) \\ -k_1 f(t - \boldsymbol{k}\cdot\boldsymbol{x}) \\ -k_2 f(t - \boldsymbol{k}\cdot\boldsymbol{x}) \end{pmatrix} \tag{39}$$

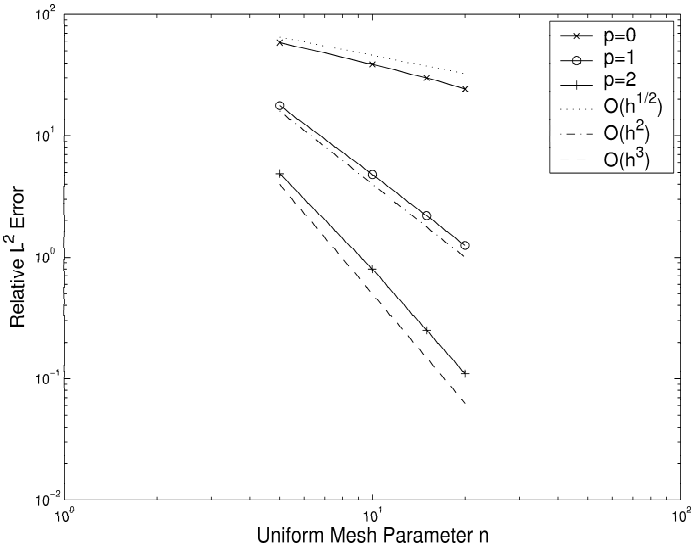

Figure 2: Relative discrete $(L^2(\Omega))^3$ error as a percentage against the mesh size h for the simple Gaussian plane wave problem. Note that when $p = 0$ we expect and observe $O(h^{1/2})$ error. But when $p = 1$ we see $O(h^2)$ and when $p = 2$ we see $O(h^3)$ whereas our theory predicted $O(h^{3/2})$ and $O(h^{5/2})$ respectively. This better than expected convergence rate is often seen for DG methods on uniform grids.

where $\boldsymbol{k} = (\cos(1), \sin(1))^T$ and

$$f(s) = \begin{cases} \frac{\exp(-10(s-1)^2) - \exp(-10)}{1 - \exp(-10)} & 0 \leq s \leq 2, \\ 0 & \text{otherwise.} \end{cases}$$

The initial data is $\boldsymbol{u}(t = 0) = 0$ and we impose the exact solution as Dirichlet data via $Q = 1$ on $\partial\Omega$ and $\sigma = 1$ on all faces. Using a uniform $n \times n$ grid of squares subdivided into right triangles in space, and allowing the program to create an unstructured grid in time we obtain the results shown in Figure 2. In practice we use the unstructured scheme to discretize n space-time slabs of width $2/n$ and compute the relative discrete $(L^2(\Omega))^3$ norm error defined by

$$Err(t) = \frac{\|\boldsymbol{u}_I(t) - \boldsymbol{u}_h(t)\|_\Omega}{\|\boldsymbol{u}_I(t)\|_\Omega}$$

where $\boldsymbol{u}_I$ is the standard interpolant of $\boldsymbol{u}$ from the finite element space. In this example the error is measured at $t = 2$. Apart from the case of piecewise constants ($p = 0$) we see convergence at the rate $O(h^{p+1})$ (this improved rate of convergence is known to occur for DG methods on a uniform triangular grid [14] - but because of the timestepping we have a non-uniform tetrahedral grid).

7.2 Standing wave

In this example, we have vanishing boundary data, but non-zero initial data. In addition, the time integration is carried out over a longer period than in the

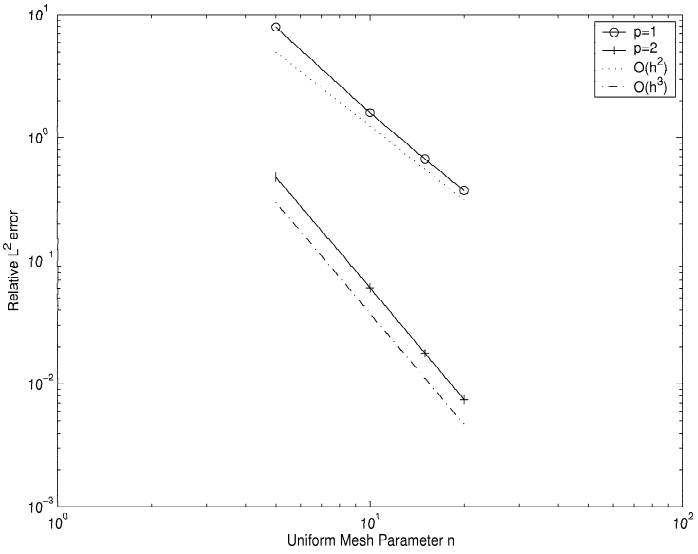

Figure 3: Relative discrete $(L^2(\Omega))^3$ error as a percentage against the mesh size h for the standing wave problem. The error is computed at a final time $t = 4$ for $p = 1, 2$. We see $O(h^2)$ and when $p = 2$ we see $O(h^3)$ convergence.

previous example. The domain is again $\Omega = [0, 2]^2$. The exact solution is now

$$\boldsymbol{u} = \begin{pmatrix} \cos(\delta t)\sin(\pi x_1/2)\sin(\pi x_2/2) \\ \pi/(2\delta)\sin(\delta t)\cos(\pi x_1/2)\sin(\pi x_2/2) \\ \pi/(2\delta)\sin(\delta t)\sin(\pi x_1/2)\cos(\pi x_2/2) \end{pmatrix}$$

with $\delta = \pi/\sqrt{2}$ which satisfies zero Dirichlet data on $\partial\Omega$ (implemented with $Q = 1$, $\sigma = 1$ and $\boldsymbol{g} = 0$). Results for a uniform $n \times n$ spatial mesh subdivided into right triangles are shown in Figure 3, and for $p = 1, 2$ (the case $p = 0$ does not produce an acceptable accuracy for the meshes and final time used in this case). Again we see convergence at a rate $O(h^{p+1})$ for $p = 1, 2$.

7.3 Penetrable cylinder

Our final test uses a non-uniform spatial grid and a variable sound speed as is usually encountered in practice. We wish to approximate the function $\boldsymbol{u}$ that satisfies (1) in $\mathbb{R}^2 \times (0, T)$ and which models an acoustic wave interacting with an inhomogeneous scatterer. In particular we assume that the coefficients α and γ in the 2D analogue of (35) satisfy $\gamma = 1$ in $\mathbb{R}^2$ and

$$\alpha = \begin{cases} \alpha_1 & \text{if } |\boldsymbol{x}| < a, \\ \alpha_2 & \text{if } |\boldsymbol{x}| > a. \end{cases}$$

For the numerical experiments we choose $a = 0.25$, $\alpha_1 = 4$ and $\alpha_2 = 1$. To complete the description of the system, we define

$$\boldsymbol{u} = \begin{cases} \boldsymbol{u}^{(1)} & \text{if } |\boldsymbol{x}| < a, \\ \boldsymbol{u}^{(2)} & \text{if } |\boldsymbol{x}| > a. \end{cases}$$

The exterior field is decomposed into the sum of a scattered field denoted $\boldsymbol{u}^{(2)s}$ and a known incident field denoted $\boldsymbol{u}^i$ so that $\boldsymbol{u}^{(2)} = \boldsymbol{u}^{(2)s} + \boldsymbol{u}^i$. The incident field satisfies the acoustic symmetric system with $\alpha = \alpha_2$ in all space and is such that $\boldsymbol{u}^i(\boldsymbol{x}, 0) = 0$ for $|\boldsymbol{x}| < a$ (i.e. it vanishes in the neighborhood of the cylinder at $t = 0$). The scattered field $\boldsymbol{u}^{(2)s}$ has compact support in space at each time and in particular $\boldsymbol{u}^{(2)s}(\boldsymbol{x}, 0) = 0$ for all $\boldsymbol{x}$. On the interface $|\boldsymbol{x}| = a$, our jump conditions are

$$D\boldsymbol{u}^{(1)} = D\boldsymbol{u}^{(2)s} + D\boldsymbol{u}^i$$

with D as in (36). Thus $[u_1] = 0$, $[u_2, u_3] \cdot \boldsymbol{n} = 0$ (equivalently, u_t and the normal component of ∇u are continuous). The incident field is taken to be a plane wave of the form (39) with $\boldsymbol{k} = (1, 0)^T$ and

$$f(s) = \begin{cases} (1 - \cos(4\pi(s-1))) & \text{if } 1 < s < 3/2, \\ 0 & \text{otherwise .} \end{cases} \tag{40}$$

This completes the specification of the acoustic scattering problem. In order to compute an approximate solution for long times we would need to use an absorbing boundary condition or other truncation condition on an auxilliary boundary. Since we do not wish to discuss absorbing boundary conditions here we approximate the scattering problem for short time as follows. We compute on the domain shown in Figure 4 and compute the total field both inside and outside the scatterer. Due to the symmetry of the problem only half of the problem needs to be computed provided a homogeneous Neumann boundary condition ($Q = -1$) is used on the lower edge.

The field is introduced at the left boundary via a non-homogeneous Neumann boundary condition and the remaining boundary conditions are homogeneous Neumann conditions (all $Q = -1$). The incident field propagates to the right until it is scattered by the cylinder. We record the field at various vertices in the computational domain. This field approximates the true scattered field until spurious reflections from the outer boundary pollute the result.

Before presenting the results of the computation, we briefly sketch how to derive an exact solution to the underlying scattering problem. In particular we shall only seek to approximate the first component u_1 of the problem. By eliminating the remaining components from the symmetric system we see that u_1 satisfies the wave equation

$$\frac{1}{c^2}\frac{\partial^2 u_1}{\partial t^2} = \Delta u_1 \quad \text{in } \mathbb{R}^2 \times (0, \infty),$$

where c is given by

$$c = \begin{cases} 1/\sqrt{\alpha_1 \gamma} & \text{if } |\boldsymbol{x}| < a, \\ 1/\sqrt{\alpha_2 \gamma} & \text{if } |\boldsymbol{x}| > a. \end{cases}$$

The decomposition of the field $\boldsymbol{u}$ into exterior and exterior fields, and into scattered and incident fields implies that $u_1^{(2)} = u_1^{(2)s} + u_1^i$. The incident field satisfies the wave equation with $c = 1/\sqrt{\alpha_2 \gamma}$ in all space and is such that $u_1^i(\boldsymbol{x}, 0) = u_{1,t}^i(\boldsymbol{x}, 0) = 0$ for $|\boldsymbol{x}| < a$ (i.e. it vanishes in the neighborhood of

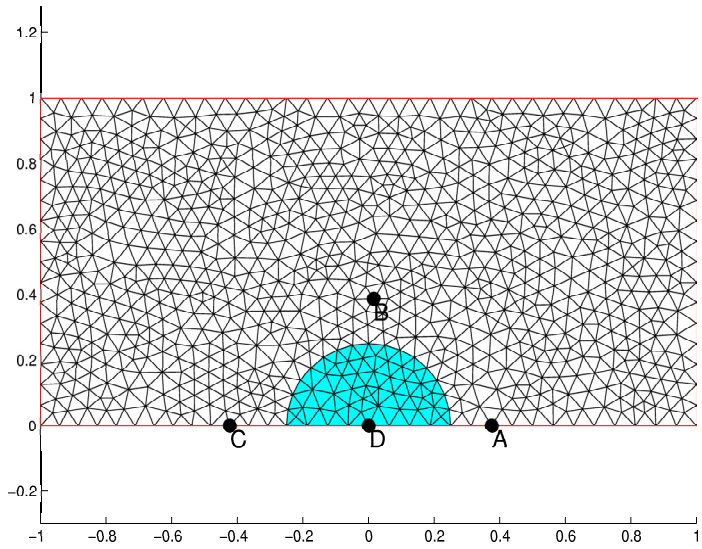

Figure 4: The mesh for the scattering problem. The scatterer is the semi-circle shaded in the grid. The outer boundary is taken far enough from the scatterer to allow the computation of the scattered field near the scatterer for a short time. The incident field is introduced along the left boundary. The output points are marked by a dot and labeled.

the cylinder at $t = 0$). The scattered field $u_1^{(2)s}$ has compact support at each time and in particular $u_1^{(2)s}(\boldsymbol{x}, 0) = u_{1,t}^{(2)s}(\boldsymbol{x}, 0) = 0$ for all $\boldsymbol{x}$. On the boundary $|\boldsymbol{x}| = a$ the continuity conditions imply that

$$u_1^{(1)} = u_1^{(2)s} + u_1^i, \tag{41}$$

$$\frac{\partial}{\partial r} u_1^{(1)} = \frac{\partial}{\partial r} u_1^{(2)s} + \frac{\partial}{\partial r} u_1^i, \tag{42}$$

where $r = |\boldsymbol{x}|$. Taking the Fourier transform in time (transformed variables are denoted by $\hat{\cdot}$) using

$$\hat{u}_1(\boldsymbol{x}, \omega) = \int_{-\infty}^{\infty} u_1(\boldsymbol{x}, t) \exp(i\omega t)\, dt$$

we see that

$$\Delta \hat{u}_1^{(1)} + \frac{\omega^2}{c_1} \hat{u}_1^{(1)} = 0 \quad \text{for } r < a,$$

$$\Delta \hat{u}_1^{(2)s} + \frac{\omega^2}{c_2} \hat{u}_1^{(2)s} = 0 \quad \text{for } r > a.$$

We are thus lead to define the wavenumbers $k_1 = \omega\sqrt{\alpha_1 \gamma}$ and $k_2 = \omega\sqrt{\alpha_2 \gamma}$. Using cylindrical polar coordinates we have the expansion (using the fact that $\hat{u}_1^{(2)s}$ is a scattered field)

$$\hat{u}_1^{(1)} = \sum_{n=\infty}^{\infty} a_n J_n(k_1 r) \exp(in\theta),$$

$$\hat{u}_1^{(2)s} = \sum_{n=\infty}^{\infty} b_n H_n^{(1)}(k_2 r) \exp(in\theta),$$

where J_n and $H_n^{(1)}$ are respectively the Bessel function of order n and Hankel function of first kind and order n.

Since the incident field is taken to be a plane wave we have

$$u_1^i = f(t - x_1)$$

for f given by (40) (since $c_2 = 1$). The Fourier transform of the incident field is

$$\hat{u}_1^i = \hat{\phi}(k_2) \exp(ik_2 x_1)$$

and using the Jacobi-Anger expansion this may be written

$$\hat{u}_1^i = \hat{\phi}(k_2) \sum_{n=-\infty}^{\infty} i^n J_n(k_2 r) \exp(-in\theta).$$

Using this expansion, the jump conditions (41)–(42) provide a system of equations for determining the coefficients $\{a_n\}$ and $\{b_n\}$. The inverse Fourier transform of $\hat{u}_1$ then gives the relevant fields at any point in space. Of course it is necessary to truncate the expansions of each field, and compute the Fourier transforms numerically.

This example falls outside the theory presented in this paper because the scatterer has a curved boundary which we approximate by a polygon. This introduces extra error into the solution which should be analyzed in the future. However the advantage of this example is that it is a standard model problem in scattering theory with an exact solution. Hence we feel that it is interesting to present the numerical results.

Although our theory only proves convergence of the method in the $L^2(\Omega)$ norm, we present the first component of the total field u_1 at four points in the domain chosen to be triangle vertices in the grid. The field value at each point is found by averaging the field from the surrounding triangles. The coordinates are as follows (see Fig. 4):

A	(0.375,0)	B	(0.0149,0.3871)
C	(-0.4231,0)	D	(0,0)

Results are shown in Fig. 5 for the mesh in Fig. 4 and for $p = 1, 2$ (we do not show the results for $p = 0$ since the mesh is too coarse in that case). These results show that our method can provide a good approximation in the presence of an inhomogeneous medium.

8 Conclusion

We have shown how to construct a space-time discontinuous Galerkin method for linear symmetric hyperbolic systems that can be time-stepped by solving only local discrete problems. Furthermore the method can take different time-steps in different parts of the domain (the maximum size of the timestep depends

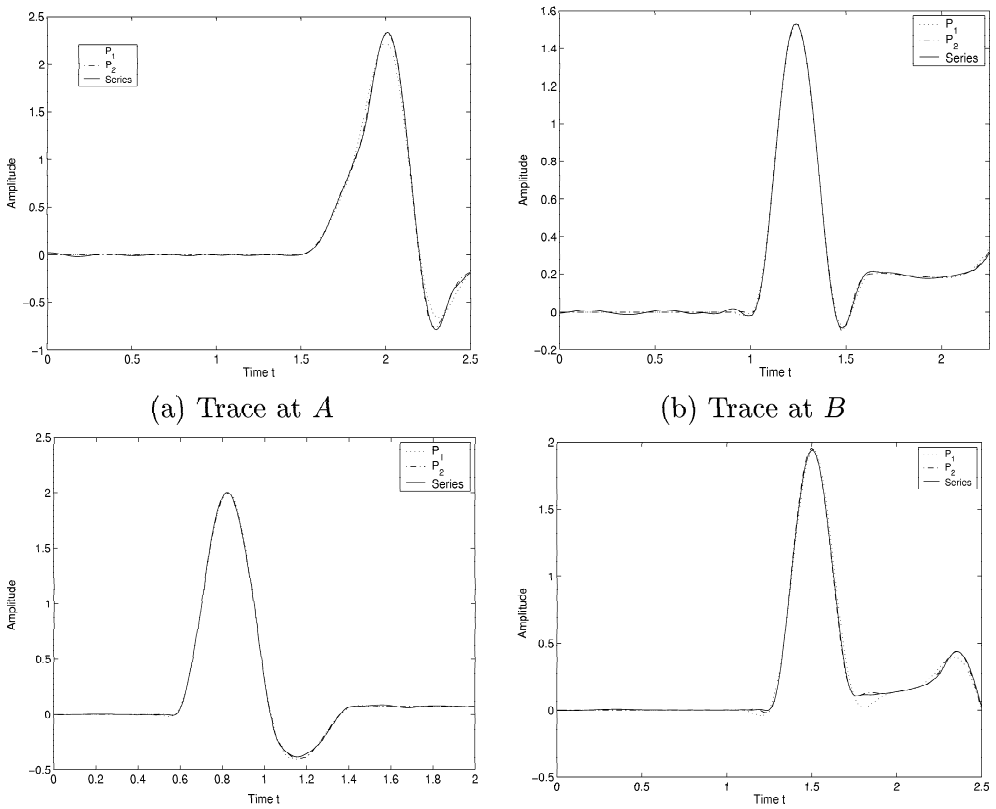

(a) Trace at A

(b) Trace at B

(c) Trace at C

(d) Trace at D.

Figure 5: Time trace of the first component of the solution at the points A, B, C and D in Figure 4. The duration of the trace is truncated to remove pollution from reflections from the outer boundary. The results for $p = 2$ are almost indistinguishable from the series solution.

on the spatial mesh size and parameter values in the equations via the requirement of outflow boundaries in the explicit ordering assumption). In addition the method can handle discontinuous material properties and rather general boundary conditions.

Disadvantages of the method are that it is dissipative due to upwinding across inter-element boundaries and that tent-pitching carries a significant overhead in time. The success of the method from [7], which is also dissipative in much the same way as is our scheme, suggests that dissipation is not necessarily fatal. Dissipation is less obvious for higher order versions of the scheme, and can be monitored a posteriori as the computation progresses (but we have not done this here). The speed of the method is also adversely influenced by the need to tent-pitch each vertex. This could be handled by precomputing the macroelements used to advance the space-time grid front for a single standard time-step from t to $t+dt$ (if $dt \approx h$ we will need to store a mesh of $O(h^{-3})$ space-time elements for a quasi-uniform grid) and so avoid repeated tent-pitching. In addition it may be desirable to use the original Falk and Richter method [5] on macroelements where the parameters of the hyperbolic system are constant.

Obviously the main question is whether our scheme can be used efficiently in three space dimensions plus time. The handling of a four dimensional tent-pitched grid is in principle possible (see [4]) and efforts to implement the scheme in this case are now underway.

Acknowledgments

The research of Peter Monk was funded by a grant from AFOSR and was carried out during visits to Rutgers University and a visit to the Isaac Newton Institute, Cambridge, England.

References

[1] B. Cockburn and C. Shu, *TVD Runge-Kutta projection discontinuous Galerkin finite element method for conservation laws II: general framework*, Math. Comput., 52 (1989), pp. 411–35.

[2] T. Driscoll and B. Fornberg, *Block pseudospectral methods for Maxwell's equations II: two-dimensional discontinuous-coefficient case*, SIAM J. Numer. Anal., 21 (1999), pp. 1146–67.

[3] B. Engquist and A. Majda, *Absorbing boundary conditions for the numerical simulation of waves*, Math. Comput., 31 (1977), pp. 629–51.

[4] J. Erickson, D. Guoy, J. Sullivan, and A. Üngör, *Building space-time meshes over arbitrary spatial domains*, in Proceedings of the 11th International Meshing Roundtable, Sandia, 2002, pp. 391–402.

[5] R. Falk and G. Richter, *Explicit finite element methods for symmetric hyperbolic equations*, SIAM J. Numer. Anal., 36 (1999), pp. 935–52.

[6] K. Friedrichs, *Symmetric positive linear differential equations*, Comm. Pure Appl. Math., 11 (1958), pp. 333–418.

[7] J. Hesthaven and T. Warburton, *Nodal high-order methods on unstructured grids - I. Time-domain solution of maxwell's equations*, J. Comput. Phys., 181 (2002), pp. 186–221.

[8] F. Hu, M. Hussaini, and P. Rasetarinera, *An analysis of the discontinuous Galerkin method for wave propagation problems*, J. Comput. Phys., 151 (1999), pp. 921–46.

[9] T. Hughes and G. Hulbert, *Space-time finite element methods for elastodynamics: formulations and error estimates*, Comput. Meth. Appl. Mech. Eng., 66 (1988), pp. 339–63.

[10] C. Johnson and J. Pitkäranta, *An analysis of the discontinuous Galerkin method for a scalar hyperbolic equation*, Math. Comput., 47 (1986), pp. 285–312.

[11] P. Lesaint and P. Raviart, *On a finite element method for solving the neutron transport equation*, in Mathematical Aspects of Finite Element Methods in Partial Differential Equations, C. deBoor, ed., Academic Press, New York, 1974, pp. 89–123.

[12] P. Monk, *A comparison of three mixed methods for the time dependent Maxwell equations*, SIAM J. Sci. Stat. Comput., 13 (1992), pp. 1097–122.

[13] W. Reed and T. Hill, *Triangular mesh methods for the neutron transport equation*, Tech. Report LA-UR-73-479, Los Alamos National Laboratory, Los Alamos, New Mexico, USA, 1973.

[14] G. Richter, *An optimal order estimate for the discontinuous Galerkin method*, Math. Comput., 50 (1988), pp. 75–88.

[15] A. Üngör and A. Sheffer, *Pitching tents in space-time: mesh generation for discontinuous Galerkin method*, International Journal of Foundations of Computer Science, 13 (2002), pp. 201–21.

[16] J.-P. Vila and P. Villedieu, *Convergence of an explicit finite volume scheme for first order symmetric systems*, Numer. Math., 94 (2003), pp. 573–602.